

Heterogeneous & Homogeneous & Bio- & Nano-

CHEM**CAT**CHEM

CATALYSIS

Accepted Article

Title: Photocatalytic decontamination of wastewater containing organic dyes by metal-organic frameworks and their derivatives

Authors: Zhibin Wu, Xingzhong Yuan, Jin Zhang, Hou Wang, Longbo Jiang, and Guangming Zeng

This manuscript has been accepted after peer review and appears as an Accepted Article online prior to editing, proofing, and formal publication of the final Version of Record (VoR). This work is currently citable by using the Digital Object Identifier (DOI) given below. The VoR will be published online in Early View as soon as possible and may be different to this Accepted Article as a result of editing. Readers should obtain the VoR from the journal website shown below when it is published to ensure accuracy of information. The authors are responsible for the content of this Accepted Article.

To be cited as: *ChemCatChem* 10.1002/cctc.201600808

Link to VoR: <http://dx.doi.org/10.1002/cctc.201600808>

WILEY-VCH

www.chemcatchem.org

A Journal of



MINIREVIEW

WILEY-VCH

Photocatalytic decontamination of wastewater containing organic dyes by metal-organic frameworks and their derivatives

Zhibin Wu^[a,b], Xingzhong Yuan^{[a,b]*}, Jin Zhang^[a,b], Hou Wang^{[a,b]*}, Longbo Jiang^[a,b], Guangming Zeng^[a,b]

Abstract: The photoactive metal–organic frameworks (MOFs) have newly emerged as a class of crystalline porous materials, which provides an advanced platform to develop catalysts for photocatalytic decolorization of wastewater. Controllable integration of pure MOFs with other active materials creates the fabrication protocols for new multifunctional hybrids with superior photocatalytic properties of dye degradation to the individual components, and the calcination of transition-metal MOFs precursors affords a convenient and practical route for preparation of nanosized photocatalyst with novel structures and good purity. Although the applications of pure MOFs for organic pollutants decomposition have been reviewed previously, there are significant advances in diverse MOFs based composites and their derivatives for dye degradation which have rarely been reviewed. This review aims to fill this gap and discuss the various influence factors, the reaction kinetics and mechanisms on dye degradation, considering the period from 2014 to 2016. Finally, the challenges and outlooks for dye decomposition by MOFs based materials are suggested.

1. Introduction

Water pollution is a critical environmental problem worldwide facing humans.^[1] Particularly, the high level of dyestuffs production and usage causes serious pollution to the water body. The hazardous colored effluents are usually discharged from many industries such as textile, rubber, paper, leather, plastics, cosmetic and printing.^[2] Over 10,000 kinds of dyes with a total yearly production over 7×10^5 tons worldwide are reported to be commercially available and approximately 10% of dyestuffs are lost in the industrial effluents.^[3] The exposal of dye effluents into the receiving water body may cause damage to aquatic organisms and humans by mutagenic and carcinogenic effects.^[4] Moreover, most of dyes with large aromatic degree are stable and nondegradable, leading to the ineffectiveness by conventional biological treatment.^[5] Therefore, to efficiently remove dyestuffs from wastewater, many physical and chemical technologies, including ion-exchange, coagulation/flocculation, adsorption, chemical oxidation, photocatalysis, and so forth are proposed.^[6] Among them, the photocatalysis, which based on the in situ generation

of highly reactive transitory species (i.e. $\cdot\text{OH}$, $\cdot\text{O}_2^-$) for mineralization of dyes into CO_2 and H_2O , has been proved to be a desirable method with ambient operating condition, low-cost and high efficiency.^[7]

Up to date, series of semiconductor photocatalysts (such as metal oxides, chalcogenides and other metal salts) and their composites,^[6a, 7b, 8] have been developed for dyes degradation. Typically, titanium dioxide (TiO_2) has received the extensive interests due to its biological and chemical inertness, nontoxicity, cost effectiveness and strong oxidizing power under UV light irradiation.^[9] Nevertheless, the large energy band gap (E_g) of TiO_2 (3.2 eV) makes it only response to no more than 4% solar spectrum of UV light, which limits its adsorption of visible light and restricts its practical application.^[8c, 10] Another type semiconductor, metal sulfides, such as CdS , In_2S_3 , Sb_2S_3 , CoS_2 , etc., have also been regarded as promising catalysts owing to high response to visible light with proper positioning of the valence and conduction bands.^[11] However, there still exists some drawbacks. The core problem of photocorrosion, which is attributed to the oxidation of sulfide ions by photogenerated holes, would also result in the secondary pollution of heavy metal ions. Besides, the low photocurrent quantum yield resulting from the high recombination of electron-hole pairs, and the catalyst agglomeration caused by high surface energy are the main deficiencies.^[9a] Therefore, it is still a great challenge to develop new photocatalysts with high efficient solar utilization for decolorization of wastewater.

Metal–organic frameworks (MOFs), a newly developed type of porous coordination polymers, is built from metal ions and/or metal-containing clusters linked by organic bridging ligands.^[12] Owing to its easy tunability of pore size and shape, large internal surface areas and a wide diversity of metallic centers, the MOFs have attracted grumous interests in adsorption,^[11a, 13] catalysis,^[14] optoelectronic devices,^[15] gas storage and separation,^[16] and drug delivery.^[17] Most importantly, recent progresses have shown that various kinds of MOFs exhibit attractive charge separation properties under light illumination through integrating different molecular functional components to harvest light.^[18] Based on the photoelectric response behavior, the MOFs have been applied to the organic pollutants photodegradation,^[11a, 19] Cr^{6+} photoreduction,^[20] photocatalytic hydrogen and oxygen production^[21] and so on.^[17, 22] In fact, the MOFs used as photocatalysts can be categorize as follows: (i) MOFs exhibit direct catalytic activity resulting from their catalytically active organic linkers or unsaturated metal centers.^[23] (ii) MOFs act as the charge carrier transporting systems through the photoexcitation of organic linkers or metal clusters;^[24] Similar to the semiconductors, MOFs also contain conduction and valence bands, which corresponds to the empty outer orbitals of metal centers and the outer orbitals of organic components, respectively.^[21b, 25] Compared to traditional inorganic photocatalysts, the light absorption capacity of photosensitive MOFs is more tailorble, due to the abundant choice of organic bridging linkers and metal centers during the design of MOFs structures and functionalities. The MOFs can be constructed

[a] Dr Zhibin Wu, Prof Xingzhong Yuan, Dr Jing Zhang, Dr Hou Wang, Dr Longbo Jiang, Pro Guangming Zeng
College of Environmental Science and Engineering
Hunan University
Changsha 410082, P.R. China
E-mail: yxz@hnu.edu.cn (X.Z. Yuan) and
huankewanghou024@163.com

[b] Dr Zhibin Wu, Prof Xingzhong Yuan, Dr Jing Zhang, Dr Hou Wang, Dr Longbo Jiang, Pro Guangming Zeng
Key Laboratory of Environment Biology and Pollution Control
Hunan University
Ministry of Education, Changsha 410082, P.R. China

Supporting information for this article is given via a link at the end of the document.

and functionalized by versatile strategies including vapor diffusion, solvothermal, emulsion precipitation, and sonication routes.^[14b] The well-defined MOFs crystalline favors the characterization for evaluation of the relationships between their structure and photocatalytic property.

However, many MOFs tend to have modest hydrolytic and undesirable thermal stabilities. Meanwhile, the performance of MOFs in photocatalysis is not comparable to that of inorganic semiconductors due to the relatively low solar energy conversion and charge separation efficiency.^[20a, 26] Fortunately, the incorporation of various kinds of functional materials into MOFs have been proposed recently, which keeps the advantages of both components, meanwhile overcomes the shortcomings during dye degradation.^[27] Moreover, the MOFs can be used as new precursors to conveniently produce nanosized transition-metal semiconductors or their hybrids for dyes degradation. Thanks to the tailorabile structure of the MOFs precursors, the chemical composition and pore texture of resultant product can be readily adjusted.^[28] These are the rapidly developing research areas. To date, many literatures have reviewed the synthesis and applications of MOFs based materials in the water splitting, CO₂ reduction, Cr⁶⁺ reduction and organic transformations.^[14b, 17-18, 29] Actually, before 2014, numerous pure MOFs were developed for photodegradation of dyestuffs wastewaters, which has been well appointed by Wang et al.,^[2b] but only few MOFs based composites or their derivatives, such as copper doped ZIF-67,^[30] Fe₃O₄@MIL-100(Fe),^[31] Pd@UiO-66(NH₂),^[32] [Cd(dcbpyno)(bix)1.5]·2H₂O/PANI,^[33] α-Bi₂Mo₃O₁₂^[34] and Bi₂MoO₆^[35] were prepared for dye degradation. Since then, the growing interest of researchers in the applicability of MOFs based composites and their derivatives for dyes photodegradation has been reflected by a high number of publications, which is rarely systematic summarized.

Therefore, this review focuses on the photocatalytic dyes (Table S1) degradation behavior of MOFs based heterojunctions and MOFs derived semiconductors, and further updates the wastewater decolorization of MOFs in the last 3 years. The factors that affect the dye degradation properties of the MOFs based photocatalysts, and the corresponding photocatalytic mechanisms have been discussed to increase the knowledge of their advantages, limitations and future challenges.

Zhibin Wu graduated with BS in Environmental Engineering from Hunan Agricultural University in 2012. Currently, he is pursuing his PhD of Environmental Science and Engineering under the guidance of Prof. Xingzhong Yuan at Hunan University, Changsha, China. His research field is the preparation and application of nanomaterials in wastewater treatment.



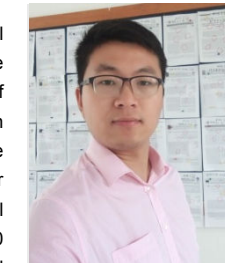
Xingzhong Yuan obtained his PhD degree from the School of Environmental Science and Engineering at Hunan University in 2003. He began his independent career in 1990 at Hunan University and was promoted to associate professor in July 1997 and professor in June 2004. His current research interests focus on waste-water processing technology and their applications, energy generation and storage, synthesis and application of adsorbents and catalysts, etc. Dr. Yuan has published over 120 papers, with citations of 2196, h-index 24



Jin Zhang obtained his BS in Environmental Engineering from Hunan Agricultural University in 2012. In 2015, he completed his a master's degree of Environmental Engineering at the Xiangtan University. Nowadays, He is a PhD student in Hunan University. He focuses on photocatalytic degradation of organic pollutants in water.



Hou Wang received his BS in Environmental Science from Jishou University in 2011. He obtained his PhD degree from the School of Environmental Science and Engineering at Hunan University in 2016. His research interests include the development of porous nanomaterials for adsorption and photocatalysis applications. Up till now, Dr. Wang has co-authored over 50 publications in peer-reviewed journals, with a total citation number of 500 and h-index of 13.



Longbo Jiang achieved his BS of Environmental Science from Hua Qiao University in 2012. He completed his Masters at Hunan University in 2015. Now, he is a PhD student at the Hunan University. He excels in the preparation of photocatalyst and its application in the phodegradation of environmental pollutants



Guangming Zeng received his PhD from Wuhan University in 1988. Later, he worked at the College of Environmental Science and Engineering, Hunan University. Now he is a professor at Hunan University and also the director of Environmental Science and Engineering. His research interests focuses on the development of novel functional materials for environmental and energy system including adsorption, catalysis, sensors, and electrochemical energy storage and conversion. Up till now, Dr. Zeng has co-authored over 840 publications in peer-reviewed journals, with a total citation number of 12950 and h-index of 56.



2. Pure MOFs photocatalysts

In the last few years, the photodegradation of organic dyes by pure MOFs have been extensively investigated.^[36] Generally, three fundamental steps are needed for the mineralization of dyes by pure MOFs photocatalyst: (i) the photosensitizers of organic linkers are excited to generate the electron-hole pair; (ii) the electrons and holes separate and transfer to the reactive

centers; (iii) the reduction and oxidation half reactions occurs with the redox equivalents (electrons and holes) at the photocatalytic centers.^[29a, 37] Photocatalytic performances of the some pure MOFs (Table 1 or Table S2) invented in the last three years for the dye degradation under UV, Visible, UV-Vis and/or sunlight irradiation are discussed in the following chapter.

Table 1 Photocatalytic performance of various MOFs monomer for the dyes degradation

MOFs	Eg (eV)	Dye	Dye and MOFs concentration (mg/L)	Additive	Light/Time for degradation (min)	Removal %	Ref.
[Cu ₃ (μ ₃ -OH)(μ-Pyz) ₃ (PDC)(H ₂ O) ₂ (CH ₃ OH)] _n	2.00	MB	12 and -	H ₂ O ₂	UV/80	92	[38]
(n-Bu ₃ Sn) ₄ Fe(CN) ₆ H ₂ O	-	MB	32 and 42	H ₂ O ₂	UV/180	100	[36c]
[GuH] ₄ [Cu ₂ ^{II} (Cit) ₂]·2H ₂ O	2.30	MO	300 and 2000	None	UV/225c	49 ^a	[39]
[Cu ^{II} LP ₄ (H ₂ O) ₄][α-Mo ₈ O ₂₆] ⁴⁻ ·4H ₂ O	-	RhB	-	None	UV/90	85	[40]
[Yb(O)(HL) ₂ (H ₂ L) _{0.5} (H ₂ O) ₃][SiMo ₁₂ O ₄₀]·2.5CH ₃ CN·1.5H ₂ O	-	RhB	-	None	UV/90	92	[41]
[Co ₂ (u ₄ -ad)0.5(HL) ₂]·(OH)·(H ₂ O)	-	RhB	-	None	UV/70	85	[42]
[NiL ₄ V ^{IV} W ^V ₁₀ W ^V ₂ O ₄₀ (V ^{IV} O) ₂]	-	MB	10 and 100	None	UV/180	96	[43]
[NiL ₄ V ^{IV} W ^V ₁₀ W ^V ₂ O ₄₀ (V ^{IV} O) ₂]	-	RhB	10 and 100	None	UV/180	88	[43]
[(Cd(tpcb)(NO ₃)(H ₂ O) ₂)(NO ₃) _n	3.24	MO	100 and 500	None	UV/270	94 ^a	[44]
[(Cd ₂ (tpcb)(SO ₄) ₂ (H ₂ O) ₆)·2MeOH·3H ₂ O] _n	2.68	MB	500 and 500	None	UV/90	92 ^a	[44]
[(Cd(tpcb) _{0.75} (OH)(H ₂ O) ₂)(NO ₃) _n	3.1	RhB	140 and 500	None	UV/180	95 ^a	[44]
[Cu ^I ₅ (pz) ₆ (H ₂ O) ₄][PW ^V ₁₀ W ^V ₂ O ₄₀]	-	RhB	2.4 and 1000	None	UV/160	79	[45]
[(Cd ₃ L ₂ (H ₂ O) ₅)·H ₂ O] _n	3.08	MB	15 and 534	H ₂ O ₂	UV/180	89	[46]
[(Cd ₆ L ₄ (bipy) ₂ (H ₂ O) ₆)·3H ₂ O] _n	3.20	MO	13 and 534	H ₂ O ₂	UV/180	80	[46]
[(Cd(btbb) _{0.5} (btac) _{0.5} (H ₂ O))·2H ₂ O] _n	2.08	MB	15 and 330	H ₂ O ₂	UV/140	93	[47]
H[Cu ₂ (μ ₂ -OH) ₂ L ¹ (CrMo ₆ (OH) ₆ O ₁₈)] _n ·4H ₂ O	-	MB	--	None	UV/105	94	[36a]
[Co(L)(ADTZ)]·H ₂ O	-	MB	10 and 556	None	UV/180	87	[48]
[Cd(L)(ADTZ)(H ₂ O)]	-	MB	10 and 250	None	UV/180	72	[49]
[Ag ₂ (en) ₂ (AT)] _n	2.12	R6G	4.8 and 500	None	UV/43	92	[50]
[(2-PTZ) ₂ Zn(H ₂ O) ₂]	2.8	MB	16 and 800	H ₂ O ₂	UV/100	99	[51]
[PhBi ₂ CN(C ₂ H ₅) ₂ Cl] _n	-	RhB	6 and 250	None	UV/50	93	[52]
[Cu(H ₂ tpc)(1,4-bidb)] _n	-	MB	8 and 250	H ₂ O ₂	UV/120	97	[53]
[H ₂ L][CuL] _n [SiW ₁₂ O ₄₀]·2H ₂ O	2.55	MB	10 and 167	None	UV/90	90	[36d]
KH[CuL] _n [SiW ₁₁ CoO ₃₉ (H ₂ O)]·2H ₂ O	3.24	MB	10 and 167	None	UV/90	90	[36d]
[Cu ₇ (4-bpt) ₆ (CN)(H ₂ O)] _n	2.17	RhB	--	None	UV/20	93	[25]
[Cu(en) ₂ (H ₂ O)][Cu(en) ₂] ₄ (AsNb ₉ V ₇ O ₄₄)·8H ₂ O	-	MB	10 and 100	None	UV/150	94	[54]
[Cu(en) ₂ (H ₂ O)][Cu(en) ₂] ₄ H(AsNb ₈ V ₈ O ₄₄)·11H ₂ O	-	RhB	10 and 100	None	UV/150	88	[54]
[Co ₂ (tipm)(1,3-BDC) ₂]·0.5CH ₃ CN	1.38	RhB	140 and 200	None	UV/180	97	[55]
[Ag ₄ V ₄ (bpp) ₄ O ₁₂] _n ·2H ₂ O	-	MB	10 and 167	None	UV/90	85	[56]
[Pb(ttbt)(1,4-b-doa)] _n ·2nH ₂ O	2.26 ^a	MV	10 and 200	None	UV/120	74	[57]
[Pb(ttbt)(1,4-b-doa)] _n ·2nH ₂ O	2.26 ^a	RhB	10 and 200	None	UV/120	99	[57]
[Pb(ttbt)(1,4-b-doa)] _n ·2nH ₂ O	2.26 ^a	MB	10 and 200	None	UV/120	89	[57]

[Cu(3-bpcb) _{0.5} (5-AlP)]·2H ₂ O	-	MB	10 and 667	None	UV/210	87	[58]
[Ag ₇ (pytz) ₄ [(PW ₁₂ O ₄₀)]	-	RhB	4.8 and 100	None	UV/80	90	[59]
[Ag ₇ (pytz) ₄ [(PW ₁₂ O ₄₀)]	-	MB	18.7 and 100	None	UV/80	98	[59]
[Ag ₇ (pytz) ₄ [(PW ₁₂ O ₄₀)]	-	AR	61 and 100	None	UV/80	70	[59]
[Mn(phen) ₂ (Hbptc)]·5H ₂ O	3.3	MB	--	None	UV/120	98	[60]
[Mn(phen) ₂ (H ₂ cpb)]	3.4	MB	10 and 250	None	UV/120	100	[61]
[Mn(phen) ₂ (H ₂ cpb)]	3.4	MO	30 and 250	None	UV/120	100	[61]
[(Pb(Tab) ₂ (bpe)) ₂ (PF ₆) ₄ ·1.64AgNO ₃] _n	2.46	MO	100 and 250	None	UV/50	95	[62]
[(Pb(Tab) ₂ (bpe)) ₂ (PF ₆) ₄] _n	2.51	AO7	100 and 250	None	UV/120	100	[62]
[(Pb(Tab) ₂ (bpe)) ₂ (PF ₆) ₄] _n	2.52	AO7	100 and 250	None	UV/90	100	[62]
[(Pb(Tab) ₂ (bpe)) ₂ (PF ₆) ₄ ·1.64AgNO ₃] _n	2.46	AO7	100 and 250	None	UV/30	100	[62]
[(Pb(Tab) ₂ (bpe)) ₂ (PF ₆) ₄] _n	2.51	OI	100 and 250	None	UV/100	100	[62]
[(Pb(Tab) ₂ (bpe)) ₂ (PF ₆) ₄] _n	2.52	OI	100 and 250	None	UV/120	100	[62]
[(Pb(Tab) ₂ (bpe)) ₂ (PF ₆) ₄ ·1.64AgNO ₃] _n	2.46	OI	100 and 250	None	UV/30	100	[62]
[(Pb(Tab) ₂ (bpe)) ₂ (PF ₆) ₄ ·1.64AgNO ₃] _n	2.46	OIV	100 and 250	None	UV/60	85	[62]
[(Pb(Tab) ₂ (bpe)) ₂ (PF ₆) ₄ ·1.64AgNO ₃] _n	2.46	OG	100 and 250	None	UV/40	95	[62]
[(Pb(Tab) ₂ (bpe)) ₂ (PF ₆) ₄] _n	2.51	CR	100 and 250	None	UV/30	100	[62]
[(Pb(Tab) ₂ (bpe)) ₂ (PF ₆) ₄] _n	2.52	CR	100 and 250	None	UV/18	100	[62]
[(Pb(Tab) ₂ (bpe)) ₂ (PF ₆) ₄ ·1.64AgNO ₃] _n	2.46	CR	100 and 250	None	UV/3	100	[62]
[(Pb(Tab) ₂ (bpe)) ₂ (PF ₆) ₄] _n	2.51	AR27	100 and 250	None	UV/60	100	[62]
[(Pb(Tab) ₂ (bpe)) ₂ (PF ₆) ₄] _n	2.52	AR27	100 and 250	None	UV/60	100	[62]
[(Pb(Tab) ₂ (bpe)) ₂ (PF ₆) ₄ ·1.64AgNO ₃] _n	2.46	AR27	100 and 250	None	UV/50	100	[62]
[(Pb(Tab) ₂ (bpe)) ₂ (PF ₆) ₄] _n	2.51	SY	100 and 250	None	UV/80	100	[62]
[(Pb(Tab) ₂ (bpe)) ₂ (PF ₆) ₄] _n	2.52	SY	100 and 250	None	UV/60	100	[62]
[(Pb(Tab) ₂ (bpe)) ₂ (PF ₆) ₄ ·1.64AgNO ₃] _n	2.46	SY	100 and 250	None	UV/40	100	[62]
[(Pb(Tab) ₂ (bpe)) ₂ (PF ₆) ₄] _n	2.51	AB10B	100 and 250	None	UV/60	100	[62]
[(Pb(Tab) ₂ (bpe)) ₂ (PF ₆) ₄] _n	2.52	AB10B	100 and 250	None	UV/25	100	[62]
[(Pb(Tab) ₂ (bpe)) ₂ (PF ₆) ₄ ·1.64AgNO ₃] _n	2.46	AB10B	100 and 250	None	UV/12	100	[62]
[(Pb(Tab) ₂ (bpe)) ₂ (PF ₆) ₄] _n	2.51	AB	100 and 250	None	UV/100	100	[62]
[(Pb(Tab) ₂ (bpe)) ₂ (PF ₆) ₄] _n	2.52	AB	100 and 250	None	UV/40	100	[62]
[(Pb(Tab) ₂ (bpe)) ₂ (PF ₆) ₄ ·1.64AgNO ₃] _n	2.46	AB	100 and 250	None	UV/20	100	[62]
[(Pb(Tab) ₂ (bpe)) ₂ (PF ₆) ₄] _n	2.51	ACBK	100 and 250	None	UV/50	100	[62]
[(Pb(Tab) ₂ (bpe)) ₂ (PF ₆) ₄] _n	2.52	ACBK	100 and 250	None	UV/60	100	[62]
[(Pb(Tab) ₂ (bpe)) ₂ (PF ₆) ₄ ·1.64AgNO ₃] _n	2.46	ACBK	100 and 250	None	UV/40	100	[62]
[(Pb(Tab) ₂ (bpe)) ₂ (PF ₆) ₄] _n	2.51	EBT	100 and 250	None	UV/24	100	[62]
[(Pb(Tab) ₂ (bpe)) ₂ (PF ₆) ₄] _n	2.52	EBT	100 and 250	None	UV/25	100	[62]
[(Pb(Tab) ₂ (bpe)) ₂ (PF ₆) ₄ ·1.64AgNO ₃] _n	2.46	EBT	100 and 250	None	UV/15	100	[62]
[Cd(L) _{0.5} (1,10-phen)(H ₂ O)]·2H ₂ O	3.31	RhB	4.8 and 250	None	UV/480	90	[63]
Co(C ₄₀ H ₃₆ N ₄ O ₈)·3CH ₃ OH	-	MB	6 and 333	None	UV/90	90	[64]
Ni(C ₄₀ H ₃₆ N ₄ O ₈)·3CH ₃ OH	-	RhB	6 and 333	None	UV/140	91	[64]
[Cu ₂ (L ²) ₂ (CrMo ₆ (OH) ₅ O ₁₉)(H ₂ O) ₂]·2H ₂ O	-	RhB	5 and 1111	None	UV/350	100	[65]
[Cu ₂ (L ²) ₂ (CrMo ₆ (OH) ₅ O ₁₉)(H ₂ O) ₂]·2H ₂ O	-	MB	10 and 1111	None	UV/210	91	[65]
[(Cd(L)(bdc)(H ₂ O))·H ₂ O] _n	-	CR	6 and 1000	None	UV/150	63	[66]

$[(\text{Cd}(\text{L})(\text{mip})(\text{H}_2\text{O})) \cdot \text{H}_2\text{O}]_n$	-	MO	8 and 1000	None	UV/150	61	[66]
$[(\text{Zn}(\text{L})(\text{tpd})(\text{H}_2\text{O})) \cdot \text{H}_2\text{O}]_n$	-	RhB	6 and 1000	None	UV/150	48	[66]
$[(\text{Zn}(\text{L})(\text{mip})(\text{H}_2\text{O})) \cdot \text{H}_2\text{O}]_n$	-	MB	10 and 1000	None	UV/150	56	[66]
$[(\text{Zn}(\text{L})(\text{hip})) \cdot 2\text{H}_2\text{O}]_n$	-	MO	8 and 1000	None	UV/150	61	[66]
$[\text{Cu}_3(4\text{-atrz})_8(\text{PMo}_{12}\text{O}_{40})2(\text{H}_2\text{O})_2] \cdot 2\text{H}_2\text{O}$	-	RhB	6 and 1667	None	UV/180	94	[67]
$[\text{Cu}_2(4\text{-atrz})_6(\text{SiW}_{12}\text{O}_{40})(\text{H}_2\text{O})] \cdot 6\text{H}_2\text{O}$	-	MB	6 and 1667	None	UV/60	98	[67]
$[\text{Cu}_2(4\text{-atrz})_4(\mu_2\text{-OH})(\text{CrMo}(\text{OH})_6\text{O}_{18})] \cdot 3\text{H}_2\text{O}$	-	MB	6 and 1667	None	UV/140	98	[67]
$\text{H}_2[\text{K}(\text{H}_2\text{O})_5]_2[\text{Cu}(\text{pzca})(\text{H}_2\text{O})_3]_2[\text{TeMo}_6\text{O}_{24}]$	-	MB	--	None	UV/90	93	[68]
$[\text{Cu}_{1.5}(\mu_2\text{-O})\text{TATAB}^*]$	-	MB	10 and 100	None	UV/70	99	[69]
$(\text{Me}_2\text{DABCO})_5(\text{Cu}_{15}\text{Br}_{24})\text{Br}$	3.40	MO	3.3 and 500	None	UV/150	96	[70]
$(\text{Me}_2\text{DABCO})_5(\text{Cu}_{15}\text{Br}_{24})\text{Br}$	3.40	KR	6 and 500	None	UV/150	99	[70]
$(\text{Me}_2\text{DABCO})_5(\text{Cu}_{15}\text{Br}_{24})\text{Br}$	3.40	MB	3.7 and 500	None	UV/150	72	[70]
$(\text{Me}_2\text{DABCO})_5(\text{Cu}_{15}\text{Br}_{24})\text{Br}$	3.40	RhB	4.8 and 500	None	UV/150	58	[70]
$[(\text{Cd}_2(\text{DDB})(1,3\text{-bimb})) \cdot \text{H}_2\text{O}]_n$	-	MO	8.2 and 250	H_2O_2	UV/60	100	[36b]
$[(\text{Cd}_2(\text{DDB})(1,3\text{-bimb})(\text{H}_2\text{O})_{0.5}) \cdot \text{H}_2\text{O}]_n$	-	MO	8.2 and 250	H_2O_2	UV/60	100	[36b]
$[(\text{Cu}(\text{bpy})_2)(\text{Mo}_{12}\text{O}_{34}(\text{bpy})_{12})][\text{PMo}_{12}\text{O}_{40}]_2$	-	MB	10 and 250	None	UV/80	96	[37b]
$[(\text{Zn}(\text{L1})(\text{mip})) \cdot \text{H}_2\text{O}]_n$	-	CR	--	None	UV/150	99	[71]
$[\text{Cd}(\text{phen})\text{Cl}_2]$	-	RhB	10 and 500	None	UV/240	39	[72]
$[\text{Cd}(\text{phen})(\text{cam})] \cdot \text{H}_2\text{O}$	-	MO	10 and 500	None	UV/240	69	[72]
$[\text{Mn}_2\text{L}(1,10\text{-phen})_2] \cdot \text{DMF} \cdot 0.5\text{H}_2\text{O}$	2.45	RhB	4.8 and 500	None	UV/480	56	[73]
$\text{Ni}(\text{C}_{22}\text{H}_{26}\text{N}_2\text{O}_{10}\text{S}_2) \cdot 2\text{CH}_3\text{OH}$	-	MB	6 and 333	None	UV/140	95	[74]
$[\text{Cd}(\text{NDC})(\text{biim-4})] \cdot 0.5\text{H}_2\text{O}$	3.46	MO	--	None	UV/180	92	[75]
$[\text{Cu}_2(\text{L}^2)_2(\text{CrMo}_6(\text{OH})_5\text{O}_{19})(\text{H}_2\text{O})_2] \cdot 2\text{H}_2\text{O}$	-	RhB	5 and 1111	None	Vis/350	92	[65]
$[\text{Cu}_2(\text{L}^2)_2(\text{CrMo}_6(\text{OH})_5\text{O}_{19})(\text{H}_2\text{O})_2] \cdot 2\text{H}_2\text{O}$	-	MB	10 and 1111	None	Vis/210	85	[65]
$[\text{Cu}_{1.5}(\mu_2\text{-O})\text{TATAB}^*]$	-	MB	10 and 100	None	Vis/90	86	[69]
MIL-53(Fe)	2.88	RhB	10 and 400	H_2O_2	Vis/50	62	[19]
$[(\text{Co}_2(\text{SDB})_2(\text{BITMB})) \cdot (\text{Dioxane})_3]_n$	2.11	MY	3.8 and 300	H_2O_2	Vis/180	82	[76]
$[\text{Cu}(\text{BrIP})(\text{BITMB})(\text{H}_2\text{O})]_n$	-	MY	3.8 and 300	H_2O_2	Vis/180	89	[77]
$[\text{CuH}_2\text{L}(\text{H}_2\text{O})]_n$	2.95	RhB	18.7 and 3000	H_2O_2	Vis/120	96	[78]
CuL	-	RhB	12 and 200	H_2O_2	Vis/60	89	[79]
$[\text{CdL}]^{+}[\text{H}_2\text{N}(\text{CH}_3)_2](\text{DMF})(\text{H}_2\text{O})_3$	-	RhB	4.8 and 250	None	Vis/480	48	[80]
MIL-88A	2.05	MB	37.4 and 400	H_2O_2	Vis/50	100	[37a]
$[\text{Gd}(\text{H}_2\text{O})_7][\text{Gd}(\text{H}_2\text{O})_5][\text{Co}_2\text{Mo}_{10}\text{H}_4\text{O}_{38}] \cdot 5\text{H}_2\text{O}$	-	MO	10 and 300	None	Vis/540	69	[81]
$[\text{Gd}(\text{H}_2\text{O})_7][\text{Gd}(\text{H}_2\text{O})_5][\text{Co}_2\text{Mo}_{10}\text{H}_4\text{O}_{38}] \cdot 5\text{H}_2\text{O}$	-	RhB	10 and 300	None	Vis/540	77	[81]
$[(\text{Ni}^{II}(\text{SalImCy})_2(\text{Cu}^I\text{CN})_9]_n$	1.6	MB	12 and 750	H_2O_2	Vis/22	99	[82]
$[(\text{MV})((\text{UO}_2)_2(\text{TDC})_3)]_n$	-	RhB	10 and 500	None	Vis/180	100	[83]
MIL-53(Fe)	2.72	MG	20 and 1000	Cr^{6+}	Vis/40	100	[84]
MIL-53(Fe)	2.72	RhB	20 and 1000	Cr^{6+}	Vis/40	83	[84]
$[\text{Cu}(\text{btmx})(\text{Cl})_2]_n$	2.48 ^a	MO	18 and 600	H_2O_2	Vis/140	81	[85]
$[(\text{CH}_3)_2\text{NH}_2][\text{ZnL}_2(\text{PW}_{12}\text{O}_{40})] \cdot 8\text{DMF} \cdot 14\text{H}_2\text{O}$	-	MB	10 and 750	None	Vis/17	100 ^a	[86]
$[(\text{CH}_3)_2\text{NH}_2][\text{ZnL}_2(\text{PW}_{12}\text{O}_{40})] \cdot 8\text{DMF} \cdot 14\text{H}_2\text{O}$	-	CV	10 and 750	None	Vis/24	100 ^a	[86]
$[(\text{CH}_3)_2\text{NH}_2]_3[\text{ZnL}_2(\text{BW}_{12}\text{O}_{40})] \cdot 4\text{DMF} \cdot 4\text{H}_2\text{O}$	-	CV	10 and 750	None	Vis/24	100 ^a	[86]
$[(\text{CH}_3)_2\text{NH}_2]_4[\text{ZnL}_2(\text{CoW}_{12}\text{O}_{40})] \cdot 4\text{DMF} \cdot 7\text{H}_2\text{O}$	-	CV	10 and 750	None	Vis/24	100 ^a	[86]

$[(\text{CH}_3)_2\text{NH}_2][\text{ZnL}_2(\text{PW}_{12}\text{O}_{40})]\cdot8\text{DMF}\cdot14\text{H}_2\text{O}$	-	NR	10 and 750	None	Vis/40	95 ^a	[86]
$[(\text{CH}_3)_2\text{NH}_2][\text{ZnL}_2(\text{BW}_{12}\text{O}_{40})]\cdot4\text{DMF}\cdot4\text{H}_2\text{O}$	-	NR	10 and 750	None	Vis/40	95 ^a	[86]
UiO-66(AN)	2.47	MO	20 and 100	None	Vis/90	65	[87]
$[(\text{Co}(\text{L})_2(\text{H}_2\text{O})_6)\cdot\text{H}_2\text{O}]_n$	1.86	MB	7.4 and 3333	H_2O_2	Vis/120	99	[88]
$[(\text{Co}(\text{L})_2(\text{H}_2\text{O})_6)\cdot\text{H}_2\text{O}]_n$	1.86	RhB	9.6 and 3333	H_2O_2	Vis/110	83	[88]
$[(\text{Co}(\text{L})_2(\text{H}_2\text{O})_6)\cdot\text{H}_2\text{O}]_n$	1.86	MO	6.5 and 3333	H_2O_2	Vis/110	95 ^a	[88]
$[(\text{Co}(\text{L})_2(\text{H}_2\text{O})_6)\cdot\text{H}_2\text{O}]_n$	1.86	R6G	9.6 and 3333	H_2O_2	Vis/110	65 ^a	[88]
$[(\text{Co}(\text{L})_2(\text{H}_2\text{O})_6)\cdot\text{H}_2\text{O}]_n$	1.86	CV	8.1 and 3333	H_2O_2	Vis/110	97 ^a	[88]
$[(\text{Co}(\text{L})_2(\text{H}_2\text{O})_6)\cdot\text{H}_2\text{O}]_n$	1.86	FL	6.7 and 3333	H_2O_2	Vis/110	92 ^a	[88]
$[\text{Ni}_3(\text{H}_2\text{L}_2)\cdot(\text{HL}_2)_2]\cdot(\text{OH})_3\cdot(\text{Ac})\cdot\text{H}_2\text{O}$	-	MB	10 and 100	None	Vis/120	78	[89]
$[\text{WS}_4\text{Cu}_4(\text{CN})_2(\text{pyridine})_4]_n$	-	MB	4.9 and 750	None	Vis/60	98	[90]
$[(\text{Pr}_4\text{N})(\text{WS}_4\text{Cu}_4(\text{CN})_3)]_n$	-	MB	4.9 and 400	None	Vis/180	94	[91]
$[\text{Cu}_2(\text{mpTZ})_2\text{Br}_2]\cdot\text{H}_2\text{O}$	3.10	MB	10 and 300	H_2O_2	Vis/150	99	[92]
$[\text{Co}_3(\text{BPT})_2(\text{DMF})(\text{bpp})]\cdot\text{DMF}$	2.10	RhB	24 and 1000	H_2O_2	Vis/120	90	[93]
$[\text{Ni}_2(\text{bix})(\text{aip})_2(\text{H}_2\text{O})_2]_n$	3.74	MO	10 and 37.5	$\text{Na}_2\text{S}_2\text{O}_8$	Vis/120	91	[94]
ST-MOF235	1.98	RhB	19.2 and 200	H_2O_2	Vis/40	100	[95]
HKUST-1	2.63	MG	10 and 250	None	Vis/85	98	[96]
HKUST-1	2.63	SO	15 and 250	None	Vis/85	89	[96]
$[\text{Co}(\text{H}_2\text{L})(\text{bpfp})(\text{H}_2\text{O})_2]_n$	-	MB	10 and 500	None	Vis/180	83	[97]
$[\text{Co}_{20}(\text{OH})_{24}(\text{MMT})_{12}(\text{SO}_4)_4](\text{NO}_3)_2\cdot6\text{H}_2\text{O}$	-	MO	10 and 150	None	Vis/180	52	[98]
$[\text{Co}_{20}(\text{MT})_{12}(\mu_3\text{-OH})_{23}(\mu_3\text{-O})(\text{SO}_4)(\text{CH}_3\text{O})]\cdot2\text{EtOH}$	-	MB	10 and 150	None	Vis/180	66	[98]
$[(\text{AgL})(\text{CF}_3\text{SO}_3)]_n$	2.50	MB	--	None	UV-vis/400	100	[99]
$[(\text{AgL})(\text{CF}_3\text{SO}_3)]_n$	2.50	MB	--	None	Sunlight/7980	90	[99]
$\text{H}[\text{Cu}_2(\mu_2\text{-OH})_2\text{L}^1(\text{CrMo}_6(\text{OH})_6\text{O}_{18})]\cdot4\text{H}_2\text{O}$	-	MB	--	None	Sunlight/780	87	[36a]
$[\text{Cu}_2\text{L}^2(\text{CrMo}^{\text{VI}}_5\text{Mo}^{\text{V}}(\text{OH})_6\text{O}_{18})(\text{H}_2\text{O})_4]\cdot4\text{H}_2\text{O}$	-	MB	--	None	Sunlight/780	83	[36a]
$\text{H}_2[\text{K}(\text{H}_2\text{O})_5]_2[\text{Cu}(\text{pzca})(\text{H}_2\text{O})_3]_2(\text{TeMo}_6\text{O}_{24})$	-	MB	--	None	Sunlight/150	88	[68]
$[\text{Zr}^{IV}_6\text{O}_4(\text{OH})_4(\text{CO}_2)_{12}]$	2.88	MB	100 and 667	None	UV-vis/180	100	[23b]
$[\text{Zr}^{IV}_6\text{O}_4(\text{OH})_4(\text{CO}_2)_{12}]$	2.88	MO	100 and 667	None	UV-vis/180	83	[23b]
$[\text{Cd}(\text{dtba})(\text{bpp})]_n$	2.92	RhB	10 and 800	None	Sun-light/120	85	[100]
$\text{Cd}_8\text{S}(\text{SPh})_{14}(\text{DMF})_3$	3.08	RhB	20 and 2000	None	UV-vis/180	92 ^a	[101]
$[\text{Cd}_8\text{S}(\text{SPh})_{14}(\text{DMF})(\text{bpy})]_n$	2.80	RhB	20 and 2000	None	UV-vis/180	95	[101]
$[\text{Cd}_8\text{S}(\text{SPh})_{14}(\text{DMF})(\text{bpy})]_n$	2.80	MB	16 and 2000	None	UV-vis/180	95	[101]
UiO-66(1.25Ti)	2.47	MB	10 and 1000	None	Sun-light/80	82	[102]
$[(\text{CH}_3)_2\text{NH}_2]\cdot[\text{Cu}_2(\text{CN})_3]$	2.40	MB	3.7 and 100	None	Sunlight/1440	91	[103]
$[(\text{CH}_3)_2\text{NH}_2]\cdot[\text{Cu}_2(\text{CN})_3]$	2.40	RhB	24 and 100	None	Sunlight/1920	92	[103]

Pyz = 1H-pyrazole, PDC = 3,4-pyridinedicarboxylic acid; [38] GuH = monoprotonated guanidine, Cit = citrate anion; [39] Lp = 1,4-bppmb; [40] L = 1,4-bis(pyridinil-4-carboxylato)-1,4-dimethylbenzene; [41] L [42] = 2,6-di-(5-phenyl-1H-pyrazol-3-yl)pyridine = L₂ in ref [89], L = 1,4-bis(imidazol-1-ylmethyl)benzene [36d, 43][36d] = 1,4-bim in ref [36b]; tpcb = tetrakis(4-pyridyl)cyclobutane; [44] pz = pyrazine; [45] L = 3,4-bi(4-carboxyphenyl)-benzoic acid, bipy = 4,4'-bipyridine; [46] btec = 1,2,4,5-benzenetetracarboxylate, bptc = 3,3',4,4'-benzophenone tetracarboxylic acid; [47, 60] L = 2,3-bis(6'-methyl-2,2'-bipyridin-6-yl)pyrazine; [99] L¹ [36a] = N,N'-bis(3-pyridinecarboxamide)-piperazine = bpc in ref [58], L=3-pyridylnicotinamide, ADTZ=2,5-(s-acetic acid)dimercapto-1,3,4-thiadiazole; [48-49] en = ethylenediamine, AT = 5,5-azotetrazolate; [50] PTZ = 2-pyridyltetrazolato; [51] tptc = terphenyl-3,3',5,5'-tetracarboxylic acid, bidb = 1,4-bis(1-imidazol-1-yl)-2,5-dimethyl benzene; [53] 4-bpt = 3,5-bis-(4-pyridyl)-1,2,4-triazole; [25] tipm = tetrakis[4-(1-imidazolyl)phenyl]methane; [55] bpp = 1,3-bis(4-pyridyl) propane; [56, 93, 100] bdoa = benzene-1,4-dioxyacetic acid, ttbt = 10,11,12,13-tetrahydro-4,5,9,14-tetraaza- benzo[b]triphenylene; [57] bpy = 2,2'-bipyridine, pytz = 4-(1H-tetrazol-5-yl)pyridine; [37b, 59] phen = 1,10-phenanthroline; [60, 72] cpb = 1,3-(3',4'-carboxyphenoxy)benzene; [61] TabH = 4-(trimethylammonio)benzenethiol, bpe = 1,2-bis(4-pyridyl)ethylene; [62] L = bis-(3,5-dicarboxyphenyl)terephthalamide; [63, 73, 80] L² = N,N'-bis(3-pyridinecarboxamide)-1,3-propane; [65] L = N,N'-bis(pyridine-3-yl)-5-methylisophthalic dicarboxamide, tpd = 2,5-thiophenedicarboxylic acid, mip = 5-methylisophthalic acid, hip = 5-hydroxyisophthalic acid; [66] atrz = 4-amino-1,2,4-triazole; [67] pzca = 2-pyrazine carboxylic acid; [68] TATAB* = 4,4'-(6-(dimethylamino)-1,3,5-triazine-2,4-diyl)bis(azanediyl) dibenzoic acid; [69] bmib = 1,3-bis(2-methylimidazol-1-ylmethyl)benzene; [36b] cam = camphoric acid; [72] C₂₂H₂₆N₂O₁₀S₂ = 1,2-bis(2-methoxy-6-formylphenoxy)ethane-2-aminoethane-sulfonic acid; [74] biim-4 = 1,4-

bis(1-imidazolyl) butyric alkyl, NDC = 1,4-naphthalene dicarboxylic acid; ^[75] SDB = (4,40-sulfonyldibenzoate), BITMB = (1,3-bis(imidazol-1-ylmethyl)-2,4,6-trimethyl benzene); ^[76] BrIP = 5-bromoisonphthalate; ^[77] L = 5-[2-carboxy-3-(1H-tetrazol-5-yl)-phenoxy]-isophthalic acid; ^[78] L = 1,2-phenylenediamine-N,N-bis(3-tert-butyl-5-(4-pyridyl)salicylidene); ^[79] TDC = thiophene-2,5-dicarboxylate; ^[83] btmx = 1,4-bis(1,2,4-triazole-1-methylene)-2,3,5,6-tetramethyl benzene; ^[85] L = 1,1'-methylenebis(3-(4-carboxyphenyl)-1H-imidazol-3-iium); ^[86] L = 1-aminobenzene-3,4,5-tricarboxylic acid; ^[88] L₁ = 2,6-bis(benzimidazol-2-yl)pyridine; ^[89] mpTZ = N-methyl-4-pyridinium tetrazolate; ^[92] BPT = biphenyl-3,4,5-tricarboxylic acid; ^[93] bpfp = bis(4-pyridylformyl)piperazine; ^[97] MMT = 2-mercapto-5-methyl-1,3,4-thiadiazole; ^[98] dtba = 2,2'-dithio-dibenzonic acid; ^[100]^a Values estimated from original figures of the references

Compared with traditional inorganic semiconductors, the huge advantage of MOFs for dye degradation is the excellent tunability optical properties by changing or modifying the organic linker and the metal centers. For example, the so-called secondary building unit (SBU) concept, which involves the identification of a robust and reproducible building block as a vertex and subsequently construction of a network by linking them with organic ligands of well-defined geometry, is an effective route to synthesize and design the MOFs. ^[38, 93] Based on the pyrazole-based functional MOFs, Bala and co-workers have developed three Cu(II) MOFs of $[(\text{Cu}_3(\mu_3-\text{O})\text{H})(\mu-\text{Pyz})_3(\text{NAPH})]\text{DMF}\cdot\text{H}_2\text{O}\cdot\text{CH}_3\text{OH}]_n$ (MOF-1), $[\text{Cu}_3(\mu_3-\text{OH})(\mu-\text{Pyz})_3(\text{BIPH})\text{(H}_2\text{O})_2]_n$ (MOF-2), and $[\text{Cu}_3(\mu_3-\text{OH})(\mu-\text{Pyz})_3(\text{PDC})\text{(H}_2\text{O})_2]\text{(CH}_3\text{OH})_n$ (MOF-3) using the multinuclear Cu-pyrazolate system as an SBU by a solvothermal method under similar conditions, where Pyz = 1H-pyrazole, NAPH = 1,4-naphthalenedicarboxylic acid, BIPH = biphenyl-4,4'-dicarboxylic acid, and PDC = 3,4-pyridinedicarboxylic acid. ^[38] It is found that the three MOFs have the intriguing structural networks like (4, 4) type herringbone grid or an archetypal Kagome topology, and the planar Cu-pyrazolate moiety with open metal sites or loosely bound solvent molecule offers an excellent platform for photocatalysis. The band gap energies of MOF-1, MOF-2, and MOF-3 are calculated to be 3.87, 2.03, and 2.00 eV, respectively. Such band-gap sizes of MOFs 1-3 imply that the samples may have potential in response to light for photocatalytic reactions. The MOF-3 exhibits higher methylene blue (MB) and methyl Orange (MO) photodegradation efficiency than MOF-1 and MOF-2 under UV irradiation with H_2O_2 addition due to the discrepancy of their energy band gap (E_g) resulting from the structural difference.

To investigate in depth the effect of polynuclear complexes on photocatalytic dyes degradation, Liu and co-workers have designed and synthesized coordination complexes containing Cd^{II} clusters using auxiliary ligands of 1,1'-(1,6-hexane)bis(2-methylbenzimidazole) (hbmb), 1,4-bis(2-(4-thiazolyl)benzimidazole-1-ylmethyl)benzene (btbb), and 4,4'-bipyridine (4,4-bipy) by heating the mixture of $\text{Cd}(\text{NO}_3)_2\cdot 4\text{H}_2\text{O}$, ligands, ethanol and H_2O at 170 °C in a 25 mL stainless steel reactor. ^[46] The four different structural polynuclear Cd^{II} complexes (Figure 1), $[(\text{Cd}_3\text{L}_2(\text{H}_2\text{O})_5)\cdot\text{H}_2\text{O}]_n$, $[(\text{Cd}_3\text{L}_2(\text{hbmb})(\text{H}_2\text{O})_2)\cdot 2.5\text{H}_2\text{O}]_n$, $[(\text{Cd}_3\text{L}_2(\text{btbb})(\text{H}_2\text{O})_2)\cdot 2\text{EtOH}\cdot 1.5\text{H}_2\text{O}]_n$ and $[(\text{Cd}_6\text{L}_4(\text{bipy})_2(\text{H}_2\text{O})_6)\cdot 3\text{H}_2\text{O}]_n$, which has the band gap value of 3.08, 3.16, 3.10 and 3.20 eV, respectively, are obtained. They are subjected to degrade the MB and MO under UV light irradiation (Figure 1). The control experiments show that the MB photocatalytic decomposition rate of these four MOFs is 88.7%, 65.9%, 85.8%, and 63.8%, respectively, after 180 min irradiation, and the corresponding MO degradation rate is about 59.8%, 47.3%, 51.4%, and 80%, respectively, after 180 min

reaction. The MB degradation rate matches with the order of the band gaps, while the MO degradation of $[(\text{Cd}_6\text{L}_4(\text{bipy})_2(\text{H}_2\text{O})_6)\cdot 3\text{H}_2\text{O}]_n$ has deviated from this order. Upon the light irradiation, the electrons (e^-) of Cd^{II} complexes are excited from the valence band (VB) to the conduction band (CB) and thus the equal number of holes (h^+) with high oxidation activity are formed in the VB. Then, O_2 or hydroxyl (OH^-) adsorbed on the surfaces of Cd^{II} complexes could interact with the electrons (e^-) on the CB or the hole (h^+) on the VB, respectively, which probably form the hydroxyl radicals ($\cdot\text{OH}$). Later on, the $\cdot\text{OH}$ radicals with oxidation potential of 2.8 eV can effectively destroy the MB or MO or convert them into simple harmless compounds. ^[47] In these four species, the cooperation of dinuclear Cd^{II} clusters and tetranuclear Cd^{II} clusters in $[(\text{Cd}_6\text{L}_4(\text{bipy})_2(\text{H}_2\text{O})_6)\cdot 3\text{H}_2\text{O}]_n$ perhaps play a beneficial role in the MO degradation process. Besides, the different structures that "V"-shaped MB involves a basic group, whereas the linear MO includes a basic group and an acidic group, which affects the formation of the $\cdot\text{OH}$ radicals, and further trigger the different degradation rate. Therefore, the cluster complexes containing different kinds of nuclei may exert a different impact on the degradation of disparate organic dyes.

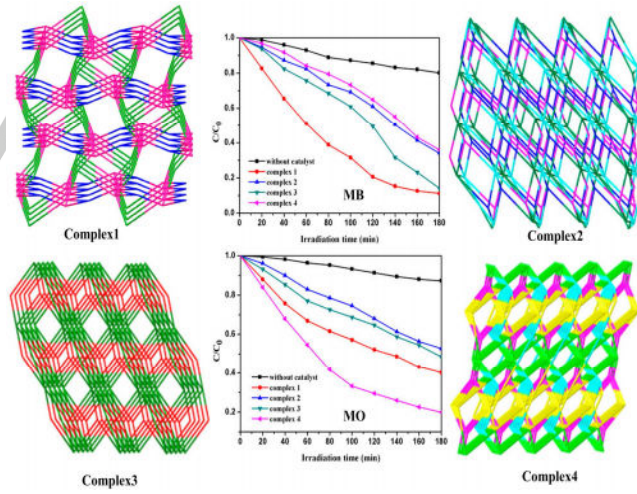


Figure 1- Crystal structures of $[(\text{Cd}_3\text{L}_2(\text{H}_2\text{O})_5)\cdot\text{H}_2\text{O}]_n$ (complex 1), $[(\text{Cd}_3\text{L}_2(\text{hbmb})(\text{H}_2\text{O})_2)\cdot 2.5\text{H}_2\text{O}]_n$ (complex 2), $[(\text{Cd}_3\text{L}_2(\text{btbb})(\text{H}_2\text{O})_2)\cdot 2\text{EtOH}\cdot 1.5\text{H}_2\text{O}]_n$ (complex 3) and $[(\text{Cd}_6\text{L}_4(\text{bipy})_2(\text{H}_2\text{O})_6)\cdot 3\text{H}_2\text{O}]_n$ (complex 4), and the photocatalytic degradation of MB and MO solution under UV light irradiation with the use of complexes 1–4. ^[46] Copyright (2014) American Chemical Society.

For the purpose of making clear the influence of center metal ions on photocatalytic activity, five 2D layered isostructural coordination complexes $[(\text{M}_3(\text{L})_2(\text{H}_2\text{O})_6)\cdot\text{H}_2\text{O}]_n$,

where the M = Mn, Mn_{0.7}Co_{0.3}, Mn_{0.5}Co_{0.5}, Mn_{0.3}Co_{0.7}, and Co, respectively, are synthesized under hydrothermal of 120 °C with ligand of 1-aminobenzene-3,4,5-tricarboxylic acid (L) at pH 9 by Shao and co-workers.^[88] The optical characterizations reveal that the five complexes have similar absorption wavelengths in the UV region attributing to similar coordination configurations, but they have different maximum absorption peaks in the visible light region (450–570 nm). The application of these complexes for organic dyes degeneration under visible light irradiation indicate that although the band gaps of [(Mn₃(L)₂(H₂O)₆)·H₂O]_n and [(Co₃(L)₂(H₂O)₆)·H₂O]_n are similar, the photocatalytic efficiency of [(Mn₃(L)₂(H₂O)₆)·H₂O]_n is quite lower than that of [(Co₃(L)₂(H₂O)₆)·H₂O]_n. The reasons of the difference photocatalytic performance are considered to be: (i) the strong spin-orbital coupling interaction of [(Co₃(L)₂(H₂O)₆)·H₂O]_n allows electrons to be easily excited from the VB to the CB by electrostatic interactions, and the half-full electronic state of [(Mn₃(L)₂(H₂O)₆)·H₂O]_n makes valence electrons hard to be excited. (ii) the energy provided by visible light is sufficient to excite the electrons of [(Co₃(L)₂(H₂O)₆)·H₂O]_n, while it is inadequate for [(Mn₃(L)₂(H₂O)₆)·H₂O]_n. (iii) the Mn^{II} can inhibit the photodegradation by combining with •O²⁻ and retarding the formation of the hydroxyl radicals.

The further discussion on the effect of photocatalytic performance with different metal ions is carried out by Wei and partners based on the complexes of [Co(HL₁)₂], [Ni(HL₁)₂], and [Ni₃(H₂L₂)₂·(HL₂)₂]·(OH)₃·(Ac)·H₂O.^[89] The three complexes are fabricated by using 2,6-bis(benzimidazol-2-yl)pyridine (L₁) and 2,6-di-(5-phenyl-1H-pyrazol-3-yl)-pyridine (L₂) as ligands under hydrothermal conditions at 160 °C. For MB decomposition under visible light, the [Co(HL₁)₂] shows the lowest photocatalytic activity and [Ni₃(H₂L₂)₂·(HL₂)₂]·(OH)₃·(Ac)·H₂O with more leaving coordination sites on the Ni center possessed highest photocatalytic activity. Although the central metal of [Ni(HL₁)₂] and [Ni₃(H₂L₂)₂·(HL₂)₂]·(OH)₃·(Ac)·H₂O is the same Ni^{II}, the photocatalytic performance is not identical, which indicates that the photocatalytic process may be influenced by other factors, such as the coordination environment, the extent of the conjugation, the structures of the complexes, and the steric hindrance around the active metal centers. The photocatalytic reaction is processed based on the highest occupied molecular orbital (HOMO, the VB) and the lowest unoccupied molecular orbital (LUMO, the CB).^[42, 56, 64, 83] Under visible-light irradiation, the electrons (e⁻) in the VB are excited to the CB with holes (h⁺) left in the VB.^[39, 48, 55] The adsorbed oxygen (O₂) can accept e⁻ to form the oxygen radicals (•O₂⁻) (O₂ + e⁻ → •O₂⁻), and it further transforms into •OH active (•O₂⁻ + 2H⁺ → •OH + OH⁻). Meanwhile, the h⁺ on VB can interact with OH⁻ forming the •OH active species for dye degradation.^[39, 89]

It is well known that difference in the average particle size, morphology and surface area as well as slight structural difference could lead to the difference in band gaps (Eg), which may cause the difference in photocatalytic activity.^[51] To make clear the influence of Eg along with levels of conduction band (CB) and valence band (VB) on the speed of the photocatalytic dyes degradation, three MOFs of [Cd(NDC)(biim-4)]·0.5H₂O,

[Cd₂(TDC)₂(biim-4)₂(H₂O)₂] and [Zn₂(biim-4)₂(TDC)₂]·2.5H₂O (biim-4 = 1,4-bis(1-imidazolyl) butyric alkyl; NDC = 1,4-naphthalene dicarboxylic acid; TDC = thiophene-2,5-dicarboxylic acid) are fabricated at pH 8 under 130 °C for MO degradation.^[75] The energy gap of [Cd(NDC)(biim-4)]·0.5H₂O (3.46 eV) is less than [Cd₂(TDC)₂(biim-4)₂(H₂O)₂] (3.75 eV) and [Zn₂(biim-4)₂(TDC)₂]·2.5H₂O (3.92 eV) due to that the conjugation unit of NDC²⁻ is larger than that of TDC²⁻, which makes the π electrons more delocalized along the polymer chain. The photocatalysis of MO degradation under UV irradiation exhibits that only 30% MO is degraded in the absence of catalyst after UV-light exposure for 3 h, while 92, 88 and 82% MO is decomposed with the existence of the three catalysts, respectively, which suggests that they are active for decomposition of MO. The order of photodegradation activities follows the reverse order of their Eg. The frontier orbitals center on different aromatic rings rather than the metal centers due to the weak ability of Cd^{II} and Zn^{II} to get or lose electrons. The preferred reactive sites for oxidation-reduction locate at the organic moiety facilitating the spatial charge separation and the photocatalytic process. Therefore, an optimal photocatalyst requires not only an appropriate band gap width to absorb light for charge carriers generation, but also the ability to efficiently transfer and separate the carriers.^[63]

To better understand the reaction kinetic behavior of the dye degradation, the pseudo-first-order model ($\ln(C_0/C) = K_1 t$) is used to describe the dye photocatalytic process.^[39, 50, 57, 61, 93] For example, Zhang and colleagues have reported the [Ag(ATZ)]_n (ATZ = 5-amino-tetrazole) and [Ag₂(en)₂(AT)]_n (en = ethylenediamine, AT = 5,5'-azotetrazolate) that for Rhodamine 6G (R6G) decomposition under UV irradiation 40 min. It is found that the R6G degradation efficiency of [Ag₂(en)₂(AT)]_n (90.8%) is superior to that of [Ag(ATZ)]_n (86.3%) with the rate constant (K₁) of 3.321 h⁻¹ and 1.989 h⁻¹, respectively. Compared to [Ag(ATZ)]_n, the structure of [Ag₂(en)₂(AT)]_n contains more delocalized π electrons in ligands, which may decrease the electronic band gap of the MOFs and benefit the ligand-to-metal charge-transfer transitions. Another significant kinetic model, namely the pseudo-second-order kinetic model that is written as $1/C_{MB} = K_2 t + 1/C_{0MB}$, has also been tested to describe the reaction dynamics by some researchers. Marcinkowski and coworkers found that, when apply the [(AgL)(CF₃SO₃)]_n (L = 2,3-bis(60-methyl-2,20-bipyridin-6-yl)pyrazine) for MB degradation, a linear relationship is between 1/C_{MB} and irradiation time (t) with correlation coefficient values of 0.9762 and 0.9975 under UV-Vis and sunlight irradiation, respectively. The rate constant (K₂) of pseudo-second-order kinetic was 0.1364 m² min⁻¹ mmol⁻¹ (UV-Vis) and 0.0011 m² min⁻¹ mmol⁻¹ (sunlight), which is ten times and two times faster than the dinuclear helical complex of silver(I).^[99]

To reveal the underlying mechanisms, two possible initial routes are proposed for MB degradation by [(AgL)(CF₃SO₃)]_n in which metal ions are in a distorted tetragonal pyramidal coordination geometry. On the one hand, the formation of active radicals is related to the photo excitation of the photocatalyst.^[91] The direct absorption of photons (hv > Eg) by [(AgL)(CF₃SO₃)]_n could cause the excitation of e⁻ in the CB and

the generation of h^+ in the VB of $[(\text{AgL})(\text{CF}_3\text{SO}_3)]_n$. The e^- in the CB is captured by surface adsorbed oxygen and thus a reactive superoxide anion is formed, which eventually suppresses the recombination of photogenerated electrons and photogenerated holes. The h^+ in the VB serves as the oxidizing species for MB degradation. On the other hand, the self-sensitization of dyes is also responsible for the degradation under illumination.^[99] The MB loaded on the photocatalyst surface can absorb the photon to excited state (MB*) under visible light irradiation ($\text{MB}_{(\text{ads})} + h\nu \rightarrow \text{MB}^*_{(\text{ads})}$). The $\text{MB}^*_{(\text{ads})}$ generates and transfers the e^- to the CB of $[(\text{AgL})(\text{CF}_3\text{SO}_3)]_n$ ($\text{MB}^*_{(\text{ads})} + [(\text{AgL})(\text{CF}_3\text{SO}_3)]_n \rightarrow [(\text{AgL})(\text{CF}_3\text{SO}_3)]_n (e^-) + \text{MB}^+_{(\text{ads})}$). Then the e^- is scavenged by molecular oxygen forming the reactive superoxide anion ($[(\text{AgL})(\text{CF}_3\text{SO}_3)]_n (e^-) + O_2 \rightarrow [(\text{AgL})(\text{CF}_3\text{SO}_3)]_n + \cdot O_2^-$).

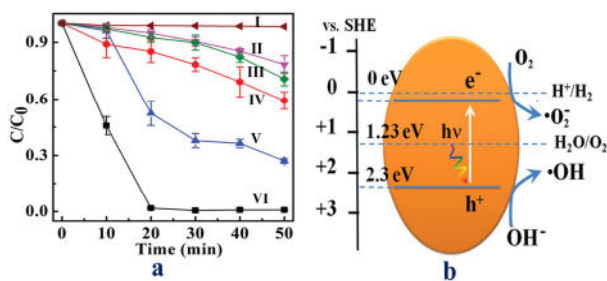


Figure 2- (a) The MB decolorization under visible light irradiation on different conditions: (I) the MIL-88A photocatalyst and H_2O_2 without light irradiation (II) MB self-decolorization; (III) $P_{25}\text{TiO}_2$ as the photocatalyst; (IV) MIL-88A as the photocatalyst; (V) only with the addition of the H_2O_2 electron acceptor; (VI) MIL-88A the photocatalyst and H_2O_2 the electron acceptor; (b) schematic illustration of the energy position of MIL-88A,^[37a] Copyright (2014) Royal Society of Chemistry.

Apparently, the former route of photocatalytic reaction critically depends on the electron–hole pairs (e^-h^+) generation and separation. The photoexcited holes either react with organic molecules directly or react with OH^- to generate $\cdot\text{OH}$ for further oxidation reaction.^[79, 92] Therefore, the e^-h^+ recombination drastically restricts the photocatalytic reaction efficiency. To suppress the e^-h^+ recombination and enhance the photocatalytic efficiency, the additives such as hydrogen peroxide (H_2O_2), potassium bromate ($KBrO_3$), sodium persulfate ($\text{Na}_2\text{S}_2\text{O}_8$) and ammonium persulfate ($(\text{NH}_4)_2\text{S}_2\text{O}_8$) are reported as the electron acceptors.^[76-77] Specially, H_2O_2 is one of the most commonly used oxidants owing to its eco-friendly nature. On one hand, the H_2O_2 can act as an electron acceptor before the recombination process of electron and hole could take place, which leads to the hydroxyl radicals generation ($H_2O_2 + e^- \rightarrow \cdot\text{OH} + OH^-$). On the other hand, the H_2O_2 can produce hydroxyl radicals under illumination by self-decomposition ($H_2O_2 + h\nu \rightarrow 2\cdot\text{OH}$). The enhanced photodegradation efficiency of MB with the addition of H_2O_2 (4×10^{-3} mol L⁻¹) is observed by Xu and co-workers, who synthesize the MIL-88A hexagonal microrods using the $\text{FeCl}_3 \cdot 6\text{H}_2\text{O}$ and fumaric acid in water at 65 °C. It is found that approximately 16% MB and less than 50% MB was degraded after 20 min visible light irradiation by using the only 400 mg/L

MIL-88A photocatalyst and only H_2O_2 , respectively (Figure 2a).^[37a] The kinetic rate constant (K) of the pseudo-first-order model for MB degradation over MIL-88A (energy position shown in Figure 2b) in the presence of H_2O_2 is 0.176 min^{-1} , which is over 17 times higher than that in the absence of H_2O_2 (0.010 min^{-1}). The synergy index (SI) calculated by $SI = K_{(H_2O_2 + \text{MIL-88A})}/(K_{H_2O_2} + K_{\text{MIL-88A}})$ is 4.7, indicating a pronounced synergic effect with the electron acceptor addition. Furthermore, the additives can be activated by transition-metal ions (i.e. Fe^{III} and Cu^{II}) to form a photo-fenton reaction or photo-fenton-like process under illumination, in which the dyes are degraded by the free radicals (i.e. $\cdot\text{OH}$ and $\cdot\text{SO}_4^{2-}$).^[19, 36c, 85, 94]

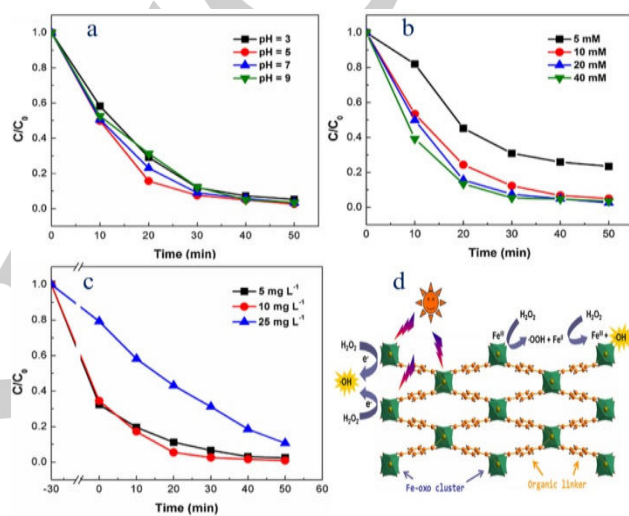


Figure 3- Effect of initial pH (a), H_2O_2 concentration (b) and dye concentration (c) on the degradation of RhB, and the proposed mechanism for the activation of H_2O_2 by MIL-53(Fe) under visible light irradiation,^[19] Copyright (2014) Elsevier.

For the purpose of activation of hydrogen peroxide (H_2O_2) to achieve high Rhodamine B (RhB) degradation efficiency in visible light, Ai and partners have synthesized the iron-based metal–organic framework MIL-53(Fe) as activator via a mild solvothermal process using $\text{FeCl}_3 \cdot 6\text{H}_2\text{O}$, terephthalic acid and dimethylformamide (DMF) at 150 °C.^[19] The 10 mg L^{-1} RhB can be completely decomposed in the binary system of H_2O_2 and MIL-53(Fe) under visible light irradiation within 50 min. The synergic effect is also found based on the pseudo-first-order kinetics constant that in the catalytic system of MIL-53(Fe)/visible light/ H_2O_2 ($7.94 \times 10^{-2} \text{ min}^{-1}$) is much higher than the sum that of MIL-53(Fe)/visible light ($1.83 \times 10^{-2} \text{ min}^{-1}$) and MIL-53(Fe)/ H_2O_2 ($1.74 \times 10^{-2} \text{ min}^{-1}$) catalytic systems. The parameters, e.g. solution pH (Figure 3a), H_2O_2 dosage (Figure 3b) and initial dye concentration (Figure 3c) significantly affect photocatalysis efficiency. The mechanisms for the synergistic effect in MIL-53(Fe)/visible light/ H_2O_2 system during the catalytic process are proposed as (Figure 3d): (i) the H_2O_2 is activated by MIL(Fe)-53 to produce $\cdot\text{OH}$ radicals through the Fenton-like reaction; (ii) the H_2O_2 captures the photogenerated

electrons in the CB of MIL-53(Fe) to form $\cdot\text{OH}$ under visible light irradiation.^[19]

To measure the stability and reusability of the pure MOFs, the MA-MOF 235, which is fabricated by microwave-assisted method at 100 °C for 30 min with $\text{FeCl}_3 \cdot 6\text{H}_2\text{O}$, terephthalic acid and DMF, is used and regenerated for the photodegradation of RhB in the $\text{H}_2\text{O}_2/\text{visible}$ system.^[95] In each cycle, the photocatalyst is reused after washing with ethanol and drying at 80 °C. It is found that the catalytic efficiency of the MA-MOF 235 remains almost unchanged after three recycles, indicating that the MOF 235 catalyst is considerably stable during the photodegradation of the RhB. The XPS spectrum indicates that the Fe 2p binding energy spectrum of MA-MOF 235 before or after repeated usages is no significant change. It is further confirmed by the atomic absorption spectrometer analysis that only a trace amount of Fe ions is detected in the centrifuged solution after three cycle usages. Besides, the recyclability of many other MOFs, like $[(\text{Pr}_4\text{N})(\text{WS}_4\text{Cu}_4(\text{CN})_3)]_n$,^[91] $[(2\text{-PTZ})_2\text{Zn}(\text{H}_2\text{O})_2]$,^[51] $[\text{CuL}]_4[\text{GeW}_{12}\text{O}_{40}]\cdot\text{H}_2\text{O}$ ^[36d] and $[(\text{MV})((\text{UO}_2)_2(\text{TDC})_3)]_n$ ^[83] are also checked by PXRD patterns or XPS spectrum.

Table 2 Photocatalytic treatment of printing-dyeing wastewater with Cr(VI) addition by MIL-53(Fe) under visible light for 10 h^[84]

Experiment condition	Discoloration removal (%)	COD-removal (%)	Cr(VI) reduction (%)
MIL-53(Fe)/pH 8	6.8	8.9	None
MIL-53(Fe)/Cr(VI)/pH 8	23.3	13.4	5.1
MIL-53(Fe)/Cr(VI)/pH 4	45.2	22.3	21.5

To simultaneously remove different categories of pollutants, Liang and coworkers have combined the MIL-53(Fe) (1000mg/L), Cr(VI) (20mg/L), and organic dyes (20 mg/L malachite green (MG) or RhB) together under visible light irradiation.^[84] For the single pollutant system, the photocatalytic efficiency of MG, RhB and Cr(VI) is about 25%, 44% and 26%, respectively, after 6 h visible light irradiation. In the binary solution of Cr(VI)/MG and Cr(VI)/RhB, the photodegradation ratio of MG and RhB is near 100% and 83%, respectively, and the reduction ratio of Cr(VI) is 70% and 66%, respectively. A synergistic effect is found between the photocatalytic reduction and oxidation process. During the catalytic process, the Cr(VI) serves as photogenerated electrons acceptor, and the MG or RhB acts as holes scavenger. The practical application of printing-dyeing wastewater (chemical oxygen demand (COD) 1340 mg/L, pH 8) shows that the addition of Cr(VI) greatly enhances the discoloration rate and the COD removal rate (Table 2). Under visible light irradiation, the iron-oxo clusters in MIL-53(Fe) adsorb incident photons and photogenerated charge carriers (e^-) with strong reduction ability ($\text{ECB} = -0.40\text{ V}$ vs. NHE at pH 6.8) transfer to the surface of the MIL-53(Fe) for the reduction of Cr(VI) to Cr(III) ($E_{\text{Cr(VI)/Cr(III)}} = +0.51\text{ V}$ vs. NHE, pH 6.8).

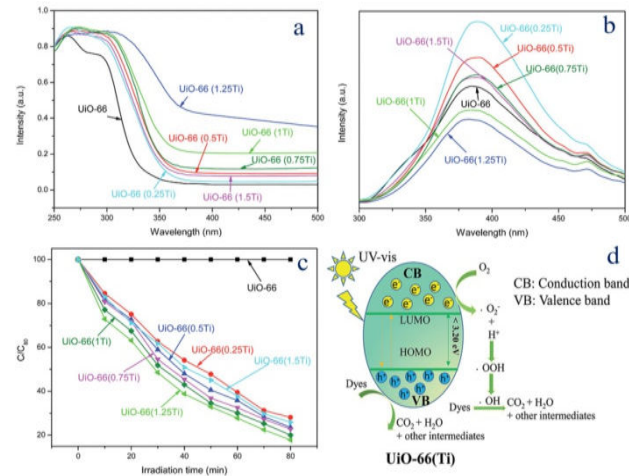


Figure 4- (a) UV-vis absorption spectra of UiO-66 and the $\text{UiO-66}(\text{Ti})$ nanocomposites with various Ti/Zr molar ratios; (b) PL spectra of UiO-66 and the $\text{UiO-66}(\text{Ti})$ nanocomposites with various Ti/Zr molar ratio; (c) Photocatalytic activity of UiO-66 and the $\text{UiO-66}(\text{Ti})$ nanocomposites with irradiation time online; (d) the proposed photocatalysis mechanism of $\text{UiO-66}(\text{Ti})$,^[102] Copyright (2016) Royal Society of Chemistry.

In order to check the feasibility of practical application, some photocatalysts are exposed on natural light or simulated sunlight for dye degradation. Xu and coworkers have used the 2-(2'-pyridyl)imidazole, CuCN, methanol, and DMF to synthesize the $[(\text{CH}_3)_2\text{NH}_2]\cdot[\text{Cu}_2(\text{CN})_3]$ by solvothermal at 140 °C for 72 h. The as-prepared $[(\text{CH}_3)_2\text{NH}_2]\cdot[\text{Cu}_2(\text{CN})_3]$ ($E_g = 2.40\text{ eV}$) is applied for the RhB and MB degradation under natural light.^[103] The photocatalytic degradation process is performed in MeOH solution with 20 mg photocatalyst 5×10^{-5} mol/L RhB and 1×10^{-5} mol/L MB. The degradation rate of RhB and MB reaches 91.4% and 91.8% at 24 h and 32 h, respectively. Wang and copartners have found that the $[\text{H}_2(\text{K}(\text{H}_2\text{O})_5)_2(\text{Cu}(\text{pzca})(\text{H}_2\text{O})_3)(\text{TeMo}_6\text{O}_{24})]$ (pzca = 2-pyrazine carboxylic acid), which is prepared by a hydrothermal method at pH 4.7 under 120 °C for 4 days, has the MB degradation efficiency of 88 % after being in sunlight for 150 min.^[68] The UiO-66 -type MOFs with oxo-bridged hetero-Zr-Ti clusters, which is synthesized via modified post-grafting method, are also applied to MB removal under simulated sun-light irradiation.^[102] After the titanium is incorporated into UiO-66 (Zr), the UV-vis absorption edges of the as-prepared $\text{UiO-66}(\text{Ti})$ nanocomposites shift to longer wavelengths, and the band gap decreasees (Figure 4a), which favors the ligand-to-metal charge transfer and visible-light region adsorption. The PL spectra (Figure 4b) shows that the $\text{UiO-66}(1\text{Ti})$ (Ti/Zr molar ratios = 1) and $\text{UiO-66}(1.25\text{Ti})$ can provide extra pathways to facilitate the electron holes separation due to existence of structural defects, which leads to the longer lifetime of the photo-generated e^-/h^+ and photocatalytic performance improvement. The $\text{UiO-66}(1.25\text{Ti})$ presents the best MB degradation efficiency of 82.2% after simulated sun-light irradiation for 80 min (Figure 4c). These indicate that the pure MOFs have great potential application in the degradation of organic dyes under sunlight irradiation. To elucidate the

photocatalytic mechanism upon irradiation using natural light or simulated sunlight, the isopropanol (1 mM) and triethylamine (1 mM) are used as the radical scavenger and the trap of superoxide, respectively. It is found that the presence of isopropanol or triethylamine depresses the MB photodegradation by UiO-66(Ti), which suggests that the radicals and superoxide are the main active species. The UiO-66(Ti) samples have the Eg less than 3.2 eV, especially, the UiO-66(1.25Ti) has an Eg about 2.47 eV. The UiO-66(Ti) can adsorb the photons (energy equal to or greater than Eg) under simulated sun-light irradiation to excite the electrons (e^-) on CB and simultaneously produce holes (h^+) on VB ($\text{UiO-66(Ti)} + h\nu \rightarrow e^- + h^+$). The excited e^- is trapped by O_2 to form $\bullet O_2^-$, which further reacts with H^+ to form $\bullet OH$. Meanwhile, the h^+ in the VB directly interacts with the OH^- to produce $\bullet OH$ ($h^+ + OH^- \rightarrow \bullet OH$). Finally, The $\bullet OH$ can attack the dye to generate CO_2 , H_2O , and other intermediates (Figure 4d).^[100, 102]

For the purpose to understand the universality or selectivity of the catalyst for dye degradation, twelve kinds of azo dyes, namely MO, Acid Orange 7 (AO7), Orange I (OI), Orange IV (OIV), Orange G (OG), Congo Red (CR), Acid Red 27 (AR27), Sunset Yellow (SY), Amido Black 10B (AB10B), Aniline Black (AB), Acid Chrome Blue K (ACBK) and Eriochrome Black T (EBT) are photodegraded under UV light by Ag(I)-doped coordination polymer $[(\text{Pb}(\text{Tab})_2(\text{bpe}))_2(\text{PF}_6)_4 \cdot 1.64\text{AgNO}_3]_n$ ($\text{Tab} = 4\text{-}(trimethylammonio)\text{benzenethiol}$, $\text{bpe} = 1,2\text{-bis}(4\text{-pyridyl)ethylene}$) which is prepared by an ambient temperature solid state reaction.^[62] The photodegradation efficiency of MO, OIV and OG are about 95%, 85% and 95% under irradiation for 50, 60 and 40 min, respectively. Meanwhile, several other dyes, AO7, OI, CR, AR27, SY, AB10B, AB, ACBK and EBT are almost completely degraded after illumination for 30, 30, 3, 50, 40, 12, 20, 40, 15 min, respectively. Such photocatalytic performance are greater than $[(\text{Pb}(\text{Tab})_2)_2(\text{PF}_6)_4]_n$ and $[(\text{Pb}(\text{Tab})_2(\text{bpe}))_2(\text{PF}_6)_4]_n$, which indicates the excellent adaptability of Ag(I)-doped coordination polymer on the elimination of various azo dyes in water. Besides, the $[(\text{Pb}(\text{Tab})_2(\text{bpe}))_2(\text{PF}_6)_4 \cdot 1.64\text{AgNO}_3]_n$ can be reused for more than five times without evident photocatalytic efficiency decay of CR and AB10B. The narrow Eg may be the reason for the higher photocatalytic activity. After the Ag^+ doped onto the network of $[(\text{Pb}(\text{Tab})_2(\text{bpe}))_2(\text{PF}_6)_4]_n$ ($Eg = 2.52$ eV), a new lower energy level (CB) can be generated between the 4d orbital of Ag^+ and the CB of $[(\text{Pb}(\text{Tab})_2(\text{bpe}))_2(\text{PF}_6)_4]_n$, which results in the Eg (2.46 eV) decrease and thus facilitates the electrons excitation for the quick generation of radical species. On the contrary, the selective photo-catalysis behavior of $(\text{Me}_2\text{DABCO})_5(\text{Cu}_{15}\text{Br}_{24})\text{Br}$ (Figure 5a and b) is observed by Yao and colleagues.^[70] The $(\text{Me}_2\text{DABCO})_5(\text{Cu}_{15}\text{Br}_{24})\text{Br}$ is prepared by heating the mixture of $CuBr_2$ (0.5 mmol), DABCO (0.30 mmol), MeOH (5 mL) and H_2O (1 mL) at 100 °C for 5 days. It is encouraged by the Eg (3.40eV), in which the VB is Cu-3d states mixing with bromine-4p states and CB is Cu-4s and Br-4s states (Figure 5c), that cuprous bromide material may be a suitable photocatalyst for the degradation of anionic dyes MO, kermes red (KR) and cationic dyes MB, RhB. The photocatalytic degradation efficiency for all tested dyes of

$(\text{Me}_2\text{DABCO})_5(\text{Cu}_{15}\text{Br}_{24})\text{Br}$ are higher than that TiO_2 (P25, Eg = 3.2 eV) and ZnO (nanorods, Eg = 3.4 eV). Notably, the degradation efficiency of the negatively charged MO (96.2%) and KR (98.8%) is far more than that of the positively charged MB (81.7%) and RhB (57.8%) (Figure 5f). The highly selective photocatalytic activity of the tubular cuprous bromide bulk crystal depends on the charge and the molecular weight of the dye, and the structure of the solid material as follow:^[43, 49, 66, 86] (i) the anionic dye selective adsorption of cationic Cu(I) sites of exposed polar faces (002) (Figure 5d and e) and the oxidation degradation of anionic pollutants is realized by the photo-induced hole on the valence bands due to that the least spatial masking of terminated Br. (ii) the effective separation of electron–hole caused by the internal fields of local dipole moments.

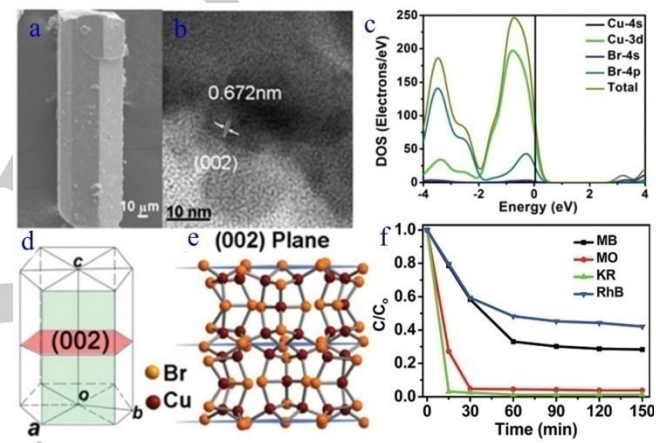


Figure 5- (a) SEM image, (b) HRTEM image, (c) calculated band gap, total density of states and the partial orbital density (d) hexagonal crystal system model, (e) Br-terminated (002) polar faces of $(\text{Me}_2\text{DABCO})_5(\text{Cu}_{15}\text{Br}_{24})\text{Br}$; (f) the selective photodegradation of p dyes in the presence of $(\text{Me}_2\text{DABCO})_5(\text{Cu}_{15}\text{Br}_{24})\text{Br}$.^[70] Copyright (2016) Royal Society of Chemistry

3. MOFs based composites photocatalysts

Since the efficiency and stability of photocatalysts for dyes reduction are not very satisfactory, it is desirable to further enhance the photocatalytic properties by integration of functional species through the formation of composites. MOFs based composites contain one MOFs and one or more distinct constituent materials, with significantly different properties from the individuals.^[24, 104] MOFs based hybrids can be fabricated either by growing or depositing of MOFs on a two-dimensional planar or curved substrate, or by incorporating MOFs with other components to form sophisticated architectures. The remarkable features of the hybrids caused by the synergistic combination of advantages (such as unique optical, electrical, catalytic properties) of both MOF and various kinds of other active components make them have excellent photocatalytic performance for dyes decomposition.^[105] To date, for dye degradation, MOFs based composites are mainly distributed in

the combination MOFs with metalliferous materials and nonmetallic carbon materials.

3.1 MOFs/ metalliferous junction photocatalysts

The MOFs with highly porous, crystalline materials provide an ideal platform for the encapsulation of catalytically active compounds as well as of photosensitizers.^[106] Furthermore, the pore-walls of the MOFs can control the nanoparticles, such as metal, metal oxide and metal salts (Table 3) particles size due to their pore sizes and large loading capacity for guest species.^[105b] Incorporating noble metal into porous matrices of MOFs to form metal@MOF nanocomposite is of hot discussion and some reports have found on the photocatalytic degradation of dyes in presence of metal nanoparticle catalysts which immobilized in MOFs. For instance, Shen and co-workers have

synthesized Pd@UiO-66(NH₂) nanocomposite via a facile one-pot hydrothermal method, to explore the photocatalytic performance for removing different categories of pollutants simultaneously.^[32] It is found that the photocatalytic activity of Pd@UiO-66(NH₂) for dyes (MO or MB) oxidation and Cr(VI) reduction in single pollutant are much higher activity than that of UiO-66(NH₂). Moreover, Pd@UiO-66(NH₂) can simultaneously photodegrade dye and photoreduce Cr(VI) with synergistic effect under visible light illumination which consumes photogenerated electrons and holes separately, thus inhibiting the recombination of photoexcited electron–hole pairs. It is commonly accepted that the noble metals with low lying Fermi energy levels can serve as reservoirs of photoelectrons, thus prolonging the lifetime of photogenerated charge carriers and enhancing the photocatalytic activity of semiconductors.

Table 3 Performance of some Metal-organic-framework/semiconductoras photocatalysts for the degradation of organic dyes

Junctions	E _g (eV)	Dye	Dye and catalysts concentration (mg·L ⁻¹)	Additive	Light/Time for degradation (min)	Removal%	Ref.
[Cd ₂ (L)(N ₃) ₄]·DMF/Bi ₂ WO ₆	2.72	MB	10 and 1000	None	UV-Vis/180	91	[107]
TiO ₂ /Cu-BTC	-	MB	7.5 and 3000	None	UV-Vis/30	95	[108]
Bi ₂ O ₃ /HKUST-1	2.70	NFR	14.3 and 0.93	None	UV/300	100	[109]
Bi ₂ WO ₆ /UiO-66-0.1	3.54 ^a	RhB	14.4 and 500	None	Vis/180	80	[110]
Bi ₂ WO ₆ /UiO-66-0.5	3.10 ^a	RhB	14.4 and 500	None	Vis/180	92 ^a	[110]
Bi ₂ WO ₆ /UiO-66-1	3.10 ^a	RhB	14.4 and 500	None	Vis/180	100 ^a	[110]
Bi ₂ WO ₆ /UiO-66-2	3.02 ^a	RhB	144 and 500	None	Vis/180	82 ^a	[110]
Agl/UiO-66(Zr)-0.1	2.86	RhB	14.4 and 500	None	Vis/60	100 ^a	[24]
Agl/UiO-66(Zr)-0.5	2.86	RhB	14.4 and 500	None	Vis/60	100 ^a	[24]
Agl/UiO-66(Zr)-1	2.86	RhB	14.4 and 500	None	Vis/60	95 ^a	[24]
Agl/UiO-66(Zr)-2	2.86	RhB	14.4 and 500	None	Vis/60	100 ^a	[24]
BiOBr/UiO-66(Zr)-0.5	2.8 ^a	RhB	14.4 and 500	None	Vis/15	94 ^a	[111]
BiOBr/UiO-66(Zr)-1	2.8 ^a	RhB	14.4 and 500	None	Vis/15	98 ^a	[111]
BiOBr/UiO-66(Zr)-2	2.8 ^a	RhB	14.4 and 500	None	Vis/15	98 ^a	[111]
BiOBr/UiO-66(Zr)-3	2.8 ^a	RhB	14.4 and 500	None	Vis/15	98 ^a	[111]
BiOBr/UiO-66(Zr)-4	2.8 ^a	RhB	14.4 and 500	None	Vis/15	95 ^a	[111]
Fe ₃ O ₄ @MIL-100(Fe)	1.80	MB	50 and 100	H ₂ O ₂	Vis/120	100	[112]
Pd/UiO-66(NH ₂)	2.76 ^a	MB	10 and 500	Cr ⁶⁺	Vis/60	78 ^a	[32]
Pd/UiO-66(NH ₂)	2.76 ^a	MO	10 and 500	Cr ⁶⁺	Vis/60	50 ^a	[32]
Ag ₂ O/Cu(tpa)(dmf)	1.42	AB92	10 and 100	None	Vis/45	100	[113]
30%Ag/AgCl@MIL-101	2.95 ^a	RhB	20 and 1000	None	Vis/18	91	[105a]
40%Ag/AgCl@MIL-101	2.95	RhB	20 and 1000	None	Vis/18	96	[105a]
50%Ag/AgCl@MIL-101	2.95 ^a	RhB	20 and 1000	None	Vis/18	78	[105a]
CdTe QD/Eu-MOF	2.29	R6G	1 and 5	None	UV/50	98	[105b]
N-K ₂ Ti ₄ O ₉ /UiO-66-NH ₂ (3:7)	-	RhB	5 and 200	None	Vis/180	90 ^a	[114]
N-K ₂ Ti ₄ O ₉ /UiO-66-NH ₂ (3:7)	-	MB	5 and 200	None	Vis/180	92 ^a	[114]
N-K ₂ Ti ₄ O ₉ /UiO-66-NH ₂ (3:7)	-	NR	5 and 200	None	Vis/180	90 ^a	[114]

Ag ₂ CO ₃ /UiO-66-0.1	3.76 ^a	RhB	14.4 and 500	None	Vis/120	88 ^a	[27a]
Ag ₂ CO ₃ /UiO-66-0.5	3.65 ^a	RhB	14.4 and 500	None	Vis/120	96 ^a	[27a]
Ag ₂ CO ₃ /UiO-66-1	3.65 ^a	RhB	14.4 and 500	None	Vis/120	97 ^a	[27a]

L = 1,4-bis(bis(3,5-dimethyl-1H-pyrazol-1-yl)methyl)benzene [107]; BTC = benzene-1,3,5-tricarboxylate [108]; ^a Values estimated from original figures of the references

Metal oxides with controllable shape, size, crystallinity and functionality are widely used in various fields, like electronics, electrochemical energy conversion and storage, solar energy harvesting, photocatalysis and so on. Some researchers have attempted to integrate metal oxides, especially those with semiconducting properties, into MOFs nanostructures. [108-109, 113] For example, TiO₂ has been immobilized in a highly porous solid matrix of Cu-BTC (BTC = benzene-1,3,5-tricarboxylate) by Binh and partners via hydrolysis of titanium (IV) isopropoxide under hydrothermal condition. This material (TiO₂@Cu₃BTC₂) exhibits high photocatalytic decomposition of MB dye, which is much better than lone TiO₂ nano-particles P25. [108] Another novel Ag₂O/MOF composite is designed by Mohaghegh and coworkers via the hydration method with AgNO₃, Cu(tpa)(dmf) and NaBH₄. The uniform assembly of Ag₂O nanoparticles on the composite surface is the visible light active ingredient. [113] In addition, by trapping the photogenerated electrons, the remained Ag in Ag₂O/MOFs can not only reduce the e⁻/h⁺ pair recombination but also prolong their lifetime. Therefore, the Ag₂O/MOF demonstrates notably high photocatalytic activity for acid blue 92 (AB92) degradation in aqueous solution. Guo and workmates have fabricated a recyclable hybrid photocatalyst of Bi₂O₃@HKUST-1 (or Bi₂O₃@Cu₃(BTC)₂) thin film by photo-decomposition of BiPh₃ loaded into the pores of HKUST-1. The Bi₂O₃@HKUST-1 exhibits a higher photochemical activity under UV illumination for nuclear fast red (NFR) degradation than the individual components, which attributes to the efficient charge-separation. After four consecutive runs, no deactivation of the photocatalyst is observed, indicating that Bi₂O₃@HKUST-1 is stable, and no decomposition or structural changes after the NFR dye photo-degradation. [109] To easily recycle the photocatalysts with convenient solid-liquid separation, the Fe₃O₄ nanoparticles with good magnetic properties are chosen for the fabrication of core-shell structures of Fe₃O₄@MOFs. As reported by Zhao and colleagues, the Fe₃O₄@MIL-100(Fe) core-shell microsphere is prepared with mercaptoacetic acid-functionalized Fe₃O₄, benzenetricarboxylic acid and FeCl₃ ethanol solution at 70 °C. [112] In the solar photocatalysis (P), Fentonlike (F), photo-Fenton-like (PF) systems, all Fe₃O₄@MIL-100 catalysts, regardless of the thickness of MOFs shell (prepared with 10, 20, and 40 cycles), exhibit more efficient degradation than pure MIL-100 (Figure 6a) for the MB degradation with H₂O₂ addition. In addition, the core-shell catalyst can be easily separated by a magnetic and reused from aqueous solution a result of the low Mr value (Figure 6b). In fact, the MB degradation efficiency with Fe₃O₄@MIL-100 is related to the thickness of the MOFs shell. Only when the outer layer is thick enough, but not too thick (optimal thickness of MOFs shell under 20 cycles about 50 nm), can the photogenerated electrons of the MOFs shell be

effectively utilized along with the holes being relayed to the core Fe₃O₄, resulting more electrons effectively reacting with H₂O₂ to generate •OH radicals (Figure 6c).

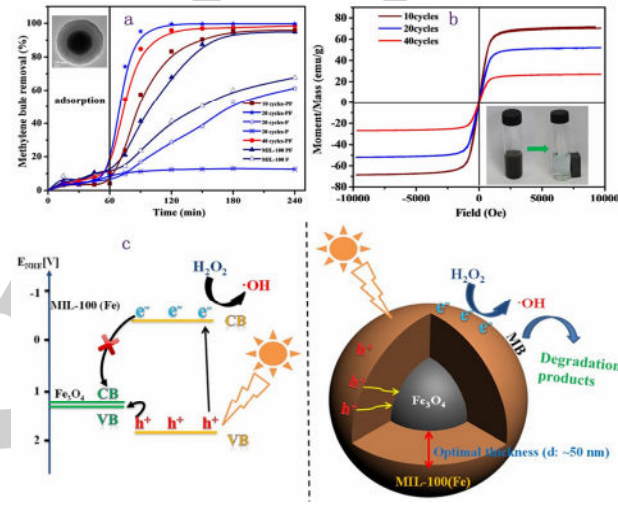


Figure 6- The magnetic hysteresis loops at room temperature (a) and photograph of the sample attracted by an external magnetic field (inset); The photodegradation of MB with different Fe₃O₄@MIL-100 prepared at given number of cycles (10, 20, and 40 cycles) with different layer thicknesses (b) and the TEM images of Fe₃O₄@MIL-100 (inset); Illustration of the possible mechanism behind the enhanced photocatalytic ability of MOFs shell with tunable thickness (c). [112] Copyright (2015) Wiley-VCH Verlag GmbH & Co. KGaA, Weinheim.

Metal salts nanomaterials composite with MOFs also can improve photocatalytic activity. There is a significant increase in the number of reports which focuses on bismuth materials and silver-based catalyst including Bi₂WO₆, BiOX, AgX, Ag₂CO₃ and so on. [8d, 107, 110-111] Currently, many metal salts/MOFs composites have been developed for dyes degradation with specially designed morphology and enhanced activity, such as [Cd₂(L)(N₃)₄]·DMF/ Bi₂WO₆, which is synthesized by Wang and coworkers using ligand of 1,4-bis(bis(3,5-dimethyl-1H-pyrazol-1-yl)methyl)benzene, Cd(NO₃)₂·4H₂O and NaN₃. It shows a better photocatalytic activity for MB degradation under Xe lamp irradiation than the pure Bi₂WO₆ and the [Cd₂(L)(N₃)₄]·DMF due to the efficient separation and reducing recombination of electrons and holes. [107] Sha and companions based on the MOFs of UiO-66(Zr), have synthesized the Bi₂WO₆/UiO-66(Zr), BiOBr/UiO-66(Zr), AgI/UiO-66(Zr) and Ag₂CO₃/UiO-66(Zr) by hydrothermal, and/or solution method for RhB decomposition. [24, 27a, 110-111] The reports show that O₂^{•-} and h⁺ are the major active species for the RhB disintegration by these four

photocatalysts, and the improved photocatalytic performance is ascribed to the promotion of the photogenerated electron–hole pairs separation. Moreover, the ratio of MOFs to metal salt affect the photocatalytic activity significantly. As illustrated in Figure 7a, among the $\text{Bi}_2\text{WO}_6/\text{UiO}-66(\text{Zr})$ (BWO/UiO-66) composites with different MOFs/metal salt ratio, the BWO/UiO-66-1 exhibits the fastest degradation rate, and RhB is almost completely degraded after 180 min.^[110] By comparing the reaction rate constants of pseudo-first-order kinetic model (Figure 7b), it can be found that there is a cooperative synergism between the Bi_2WO_6 and UiO-66 in the composites. To identify the contributors, the isopropyl alcohol (IPA), benzoquinone (BQ), and EDTA are introduced as scavengers for hydroxyl radicals ($\cdot\text{OH}$), superoxide radicals ($\text{O}_2^\bullet-$), and holes (h^+), respectively. As shown in Figure 7c, the introduction of benzoquinone (BQ) and EDTA obviously inhibits the RhB degradation, which suggests that $\text{O}_2^\bullet-$ and h^+ are the major contributors to the decomposition of RhB. The possible photocatalytic mechanism of the $\text{Bi}_2\text{WO}_6/\text{UiO}-66$ photocatalyst is proposed in Figure 7d. The photogenerated e^- in the CB of UiO-66 can react with dissolved O_2 to form $\text{O}_2^\bullet-$ and the h^+ on the VB can directly oxidize RhB. It is also reported that the photocatalytic activities of the $\text{Bi}_2\text{WO}_6/\text{UiO}-66(\text{Zr})$, $\text{BiOBr}/\text{UiO}-66(\text{Zr})$, $\text{AgI}/\text{UiO}-66(\text{Zr})$ and $\text{Ag}_2\text{CO}_3/\text{UiO}-66(\text{Zr})$ composites are primarily affected by the Bi^{3+} or Ag^+ content in the composite and the specific surface area. When ratio of Bi^{3+}/Zr or Ag^+/Zr is in the appropriate range, most of the bismuth salt or silver salt surface can be accessible and the increase content of Bi^{3+} or Ag^+ can enhance the photocatalytic activity for RhB degradation due to the formation of more active sites on the surface of the composite. Conversely, excessive Bi_2WO_6 , BiOBr , AgI and Ag_2CO_3 aggregated on the surface of UiO-66 will block the accessible pore structure and decrease the active sites.

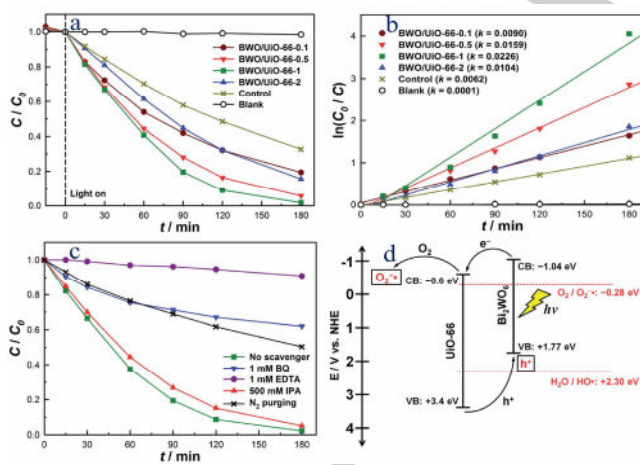


Figure 7- (a) Photocatalytic degradation of RhB in the presence and absence (blank) of different catalysts (BWO/UiO-66-0.1, BWO/UiO-66-0.5, BWO/UiO-66-1, and BWO/UiO-66-2) under visible-light irradiation. For the control experiment (mechanical mixture of pristine UiO-66 and pristine Bi_2WO_6), the amount of pristine UiO-66 or Bi_2WO_6 was equal to the actual amount of that in BWO/UiO-66-1; (b) Comparison of the reaction rate constant (k) of pseudo first-order kinetic model in the presence of different catalysts; (c) Effects of different scavengers and N_2 purging on the degradation of RhB in the

presence of BWO/UiO-66-1 under visible-light irradiation; (d) Proposed mechanism of photocatalytic degradation of RhB by the $\text{Bi}_2\text{WO}_6/\text{UiO}-66$ composite under visible-light irradiation.^[110] Copyright (2014) Royal Society of Chemistry.

Many researchers also find that some unique ternary structures also show high catalytic activity, such as $\text{Ag}/\text{AgCl}@\text{MIL}-101(\text{Cr})$, which is prepared via the vapor diffusion-photoreduction process by Gao and coworkers.^[105a] The AgCl is partial conversion to elemental Ag through the photoreduction, and the Ag/AgCl nanoparticles are homogenously dispersed on the MIL-101 with a submicrocubes structure. The photocatalytic activity of the as-prepared samples for RhB decomposition under visible light irradiation (Figure 8a) shows that the degradation efficiency of 30 wt.%, 40 wt.%, and 50 wt.% $\text{Ag}/\text{AgCl}@\text{MIL}-101$ is 90%, 96% and 80%, respectively, which is benifited from that the high specific surface area of MIL-101, the well dispersion of Ag/AgCl on MIL-101 and the enhanced optical property. The RhB decomposition in the presence of $\text{Ag}/\text{AgCl}@\text{MIL}-101$ follows the first-order kinetics (Figure 8b). The rate constant of 40 wt.% $\text{Ag}/\text{AgCl}@\text{MIL}-101$ (0.168 min^{-1}) is 16.97 times to P25, 9.18 times to the physical mixture of Ag/AgCl and MIL-101, and 3.95 times to Ag/AgCl . Such enhanced photoactivity is related to the efficient separation of photogeneration electron–hole pairs, which is testified by that the $\text{Ag}/\text{AgCl}@\text{MIL}-101$ electrode is prompt in generating stable transient photocurrent with a reproducible response to on/off cycles (Figure 8c). Upon visible light irradiation (Figure 8d), electromagnetic (EM) wave will be greatly adsorbed by Ag nanoparticles when the intrinsic frequency of electron oscillation matches with that of the light. Then h^+ and e^- are generated in the Ag NPs. The e^- is transferred to the surface of Ag nanoparticles and further transferred to the surface of MIL-101 to generate $\cdot\text{O}_2^-$ by contacting with O_2 for RhB degradation. Meanwhile, the photo induced h^+ are transferred to the surface of the AgCl , leading to the formation of Cl^0 atoms from the oxidation of Cl^- ions. The Cl^0 atoms are powerful reactive radical species that can decompose RhB and simultaneously be reduced to Cl^- for AgCl regeneration.

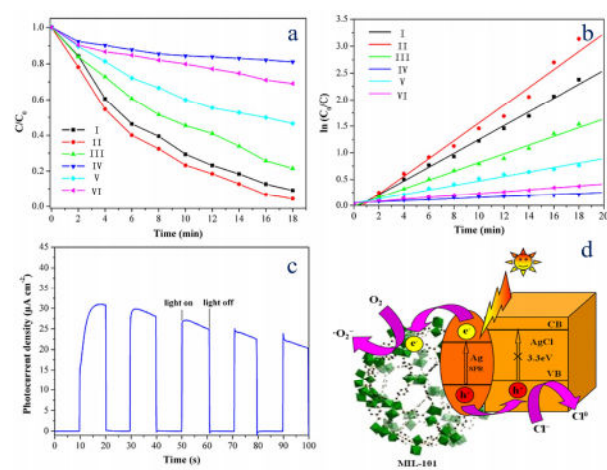


Figure 8- (a) The photodegradation of RhB with different photocatalyst. (I) 30 wt.% Ag/AgCl@MIL-101, (II) 40 wt.% Ag/AgCl@MIL-101, (III) 50 wt.% Ag/AgCl@MIL-101, (IV) P25, (V) Ag/AgCl, (VI) physical mixture of MIL-101 and AgCl; (b) The first-order kinetics of RhB degradation in the presence different samples; (c) Photoelectric conversion performances of 40 wt.% Ag/AgCl@MIL-101 in 0.1 mol L⁻¹ Na₂SO₄ aqueous solution under 300 W Xe lamp irradiation. (d) Schematic diagram for the charge separation mechanism under visible light irradiation.^[105a] Copyright (2016) Elsevier.

A remarkable form of semiconductor nanocrystals is the quantum dots (QDs) with the size range 2–10 nm. Due to their uniquely tuneable and size-dependent electronic and optical properties, the QDs have received significant attention in the photocatalysis.^[115] The wide absorption bands, narrow and symmetrical emission bands, low photobleaching, long lifetimes and high quantum yields of QDs is helpful in generating a higher redox potential in a photocatalytic system.^[105b, 116] It can harvest photons in the spectral region where the MOFs have no or little absorption. Therefore, the photon-generated excitons in the QDs can be subsequently transferred to the MOFs through resonance energy transfer. Based on this characteristic of QDs, Kaur and coworkers have synthesized the cadmium telluride (CdTe) quantum dots (QD) doped europium-MOF nanocomposite (QD/Eu-MOF) with Eg values of 2.29 eV by in-situ growth method, and applied it to degrade the R6G for the first time.^[105b] It is found that more than 98% of the dye is degraded in the solution containing 1 mg/L R6G and 5 mg/L QD/Eu-MOF within 50 min irradiation attributing to the integrative effect of the enhanced light absorption intensity, the more efficient separation of the photogenerated electron-hole

pairs, and the increased surface area. In the presence of light, the excitation of CdTe QDs and Eu-MOF generates electrons (e^-_{CB}) and holes (h^+_{VB}), respectively, for the free radical generation. The electron spin resonance (ESR) measurement shows that the holes and O_2^- radical anions are the main reactive species in the process of photocatalytic degradation of R6G. The photocatalytic process is thermodynamically favorable at low pH, and the QD/Eu-MOF has only 10% reduction in the efficiency of the R6G degradation after six cycles. These indicate the MOFs/metalliferous junction can significantly help maximize the performance of the MOFs in photodegradation of dyes.

3.2 MOFs/nonmetal hybrid photocatalysts

More recently, as the most promising candidates for functional applications, the carbonaceous materials, such as graphene family materials, carbonnitride (C_3N_4) and polymer materials have received great interesting in wastewater treatment owing to their appeal arising from the combination of the outstanding properties of in-plane graphite with a high surface area.^[13a, 117] They are regarded as the ideal building block for photocatalyst carrier and promoter.^[27b, 33, 104, 117g, 118] Proper integration of MOFs with carbonaceous materials by an appropriate strategy would further promote interfacial contact, electron-transport, sensitization for visible-light responding, generate photogenerated electrons/holes and offer more catalytic sites for target reactions. The development of MOFs/metal-free hybrid photocatalysts for dyes photodecomposition are summarized in Table 4.

Table 4 Performance of some MOFs/nonmetal hybrid as photocatalysts for the degradation of organic dyes

Hybrids	Eg(eV)	Dye	Dye and concentration ($mg \cdot L^{-1}$)	Additive	Light/Time degradation (min)	for Removal%	Ref.
rGO/MIL-125(Ti)	3.30 ^a	RhB	50 and 400	None	Vis/50	96	[117g]
Ag/rGO/MIL-125(Ti)	3.10 ^a	RhB	50 and 400	None	Vis/50	96	[117g]
MIL-101(Cr)/rGO	2.95 ^a	BG	25 and 250	None	Vis/30	80	[119]
MIL-101(Cr)/rGO	2.95 ^a	AF	25 and 250	None	Vis/30	90	[119]
Pd/MIL-101(Cr)/rGO	2.43 ^a	BG	25 and 250	None	Vis/15	100	[119]
Pd/MIL-101(Cr)/rGO	2.43 ^a	AF	25 and 250	None	Vis/20	100	[119]
MIL-101(Cr)/GO	3.87 ^a	MG	20 and 120	None	UV/60	92	[118a]
5%-rGO/NH ₂ -MIL-125(Ti)	2.48 ^a	MO	20.2 and 750	None	Vis/30	80	[120]
10%-rGO/NH ₂ -MIL-125(Ti)	3.35 ^a	MO	20.2 and 750	None	Vis/30	100 ^a	[120]
15%-rGO/NH ₂ -MIL-125(Ti)	1.82 ^a	MO	20.2 and 750	None	Vis/30	100 ^a	[120]
20%-rGO/NH ₂ -MIL-125(Ti)	1.80 ^a	MO	20.2 and 750	None	Vis/30	100 ^a	[120]
MIL-88(Fe)/GO	2.80 ^a	MB	100 and 500	None	Sunlight/50	100	[104]
MIL-88(Fe)/GO	2.80 ^a	RB	100 and 500	None	Sunlight/60	100	[104]
g-C ₃ N ₄ /MIL-125(Ti)-1	3.28	RhB	50 and 400	None	Vis/60	92 ^a	[117j]
g-C ₃ N ₄ /MIL-125(Ti)-2	3.24	RhB	50 and 400	None	Vis/60	95 ^a	[117j]

g-C ₃ N ₄ /MIL-125(Ti)-3	3.46	RhB	50 and 400	None	Vis/60	90 ^a	[117]
g-C ₃ N ₄ /MIL-125(Ti)-4	3.50	RhB	50 and 400	None	Vis/60	92 ^a	[117]
20%g-C ₃ N ₄ /MIL-53(Al)	2.60	RhB	10 and 500	None	Vis/75c	100	[27b]
PPy/ZnP ₂ Mo ₅ NR	2.92	RhB	4.8 and 250	None	Vis/120	90 ^a	[118e]
[Cu2Br(ptz)]n/Carbon Fiber (A)	2.69	RhB	4.8 and 250	None	Vis/180	58 ^a	[118d]
[Cu2Br(ptz)]n/Carbon Fiber (B)	2.46	RhB	4.8 and 250	None	Vis/180	70 ^a	[118d]
[Cu2Br(ptz)]n/Carbon Fiber (C)	2.29	RhB	4.8 and 250	None	Vis/180	90 ^a	[118d]
[Cu2Br(ptz)]n/Carbon Fiber (D)	2.02	RhB	4.8 and 250	None	Vis/180	65 ^a	[118d]
PANI/[Cd(dcbpyno)(bix) _{1.5}]·2H ₂ O	3.33	RhB	4.8 and 375	None	Vis/50	88	[33]
PANI/[CdL] ⁻ [H ₂ N(CH ₃) ₂](DMF)(H ₂ O) ₃	-	RhB	4.8 and 250	None	Vis/480	80c	[80]
MIL53(Fe)-RGO-0.5	2.72	MG	20 and 1000	None	Vis/80	22.2	[118b]
MIL53(Fe)-RGO-0.5	2.72	RhB	20 and 1000	None	Vis/80	43.0	[118b]
MIL53(Fe)-RGO-0.5	2.72	MG	20 and 1000	Cr ⁶⁺	Vis/80	100	[118b]
MIL53(Fe)-RGO-0.5	2.72	RhB	20 and 1000	Cr ⁶⁺	Vis/80	83.1	[118b]

Ppy = polypyrrole^[118e]; ptz=5-(4-pyridyl)-1H-tetrazole^[118d]; dcbpyno = 2,2'-bipyridine-3,3'-dicarboxylate-1,1'-dioxide; bix = 1,4'-bis (imidazol-1 -ylmethyl) benzene^[33]; PANI = polyaniline^[33, 80]; ^a Values estimated from original figures of the references.

Graphene (GN), a one-atom-thick two-dimensional graphitic carbon system with sp²-bonded carbon localized on a honeycomb lattice, is a zero-band gap planar material, which has high surface area and excellent electronic conductivity in storage and transport of electrons.^[4a, 117a, 121] According to the amount of oxygen containing functional groups and the degree of sp² hybrid, the member of graphene family can be categorized as graphene, reduced graphene oxide (RGO) and graphene oxide (GO). If they are as functional component incorporation with other photoactive species, the unique properties targeting at photocatalytic degradation of organic pollutants in water could be achieved due to the enhanced migration efficiency of the photoinduced electrons and reduced recombination of electron, and extended adsorption of light range.^[104, 117b] For the combination of MOFs with graphene member, it is dependent on not only the degree of oxidation, crystallite size, and the functional groups at the graphene member surface, but also the properties of MOFs, such as excellent adsorbability, encapsulation capability, high porosity and excellent photochemical properties. In previous studies, the MOFs including MIL-125(Ti),^[117g] NH₂-MIL-125(Ti),^[120] MIL-101(Cr),^[118a, 119] MIL-53(Fe),^[118b] and MIL-88(Fe),^[104] are employed in incorporation with GO/RGO by the solvothermal, photodeposition or electrostatic self-assembly method, resulting in enhanced the stability, interfacial contact action, porosity and electron-conductive properties. Indeed, the enhancement in interfacial contact plays a significant role in the photocatalytic performance improvement for the decoloration of wastewater. For examples, Liang and co-workers have reported that MIL-53(Fe) is wrapped by the curly RGO sheets via electrostatic self-assembly approach, which makes MOFs and RGO undergo a relatively abundant interfacial interaction, leading to the effective separation of photoexcited electron hole pairs. It is verified by the photoactivity of as-prepared bifunctional M53-RGO nanocomposites in the mixed systems (Cr(VI)/dyes)

under visible-light irradiation. The degradation rate of MG and RhB in the Cr(VI)/MG and Cr(VI)/RhB mixed solution is 100 and 83.1%, respectively.^[118b] Wu and coworkers have demonstrated that the Pd/MIL-101/rGO nanocomposites can afford higher photocatalytic efficiency for degradation of two triphenylmethane dyes, brilliant green (BG) and acid fuchsin (AF) than the MIL-101 and MIL-101/rGO photocatalysts under visible light.^[119] Meanwhile, they declare that the MIL-88(Fe)@GO have the superior photocatalytic efficiency for two dyes (MB and RhB) to GO and MIL-88(Fe) under exposure to natural sunlight, due to the synergistic effect between MOFs and rGO/GO.^[104] Besides, the photocatalytic activity of the composite is significantly depended on the amount of graphene member. Huang and workmates have found that the reduced graphene oxide/NH₂-MIL-125(Ti) (rGO-NMTi), which is developed by solvothermal method, has much higher photocatalytic activities than NH₂-MIL-125(Ti) for MB degradation under visible-light irradiation. But, when the rGO content increased to 20 wt%, a slight decrease in photocatalytic activity is observed. The reason is considered to be that the higher contents of rGO will result in an redundant ratio between rGO and NH₂-MIL-125(Ti), thereby weakening the electron transfer efficiency from NH₂-MIL-125(Ti) to rGO surfaces.^[120] The separation efficiency of electrons–hole pairs can further affect the generation of •O₂⁻, •OH and holes (h⁺) for dyes degradation. For an instance, Yuan and co-workers have developed the ternary system composite of Ag/rGO/MIL-125(Ti) via one-pot self-assembly and photoreduction strategy.^[117g] As shown in Figure 9a, the photocatalytic performance for RhB degradation under visible light of Ag/rGO/MIL-125(Ti) is superior to that of the binary counterparts and pure MIL-125(Ti) due to synergistic interaction between rGO and Ag. During the process, the rGO acts as efficient electron transporter and collector and the Ag nanoparticle plays as an ‘electron trap’. The pseudo first-order kinetic (Figure 9b) constant of

Ag/rGO/MIL-125(Ti) (0.0644 min^{-1}) for RhB degradation is 1.62 times higher than that of pure MIL-125(Ti) (0.0396 min^{-1}). The radical and hole trapping experiment using EDTA-2Na, *p*-benzoquinone, isopropylalcohol or nitrogen flow (Figure 9c) indicates that the RhB degradation mainly depends on $\cdot\text{O}_2^-$, $\cdot\text{OH}$ and holes (h^+). As illustrated in Figure 9d, on one hand, under visible light illumination, the interband electrons in Ag species are excited due to plasmon resonance, then the excited electrons move to MIL-125(Ti) for the reduction of Ti^{4+} to Ti^{3+} or move to rGO for the consumption of electron acceptors like O_2 . Thereafter, the reaction of Ti^{3+} with O_2 and the reaction of Ag^+ with H_2O or OH^- result in the formation of $\cdot\text{O}_2^-$ and $\cdot\text{OH}$ respectively (the Ti^{4+} and Ag species are recycled), which would directly oxidize the dye. On the other hand, the RhB adsorbed onto Ag/rGO/MIL-125(Ti) by $\pi-\pi$ conjugation can be excited to RhB * (dye photosensitization effect) and then RhB * release free electrons to MIL-125(Ti), rGO or Ag NPs. The RhB $^+$ from RhB * is finally degraded by the reactive oxygen species or holes.^[117g]

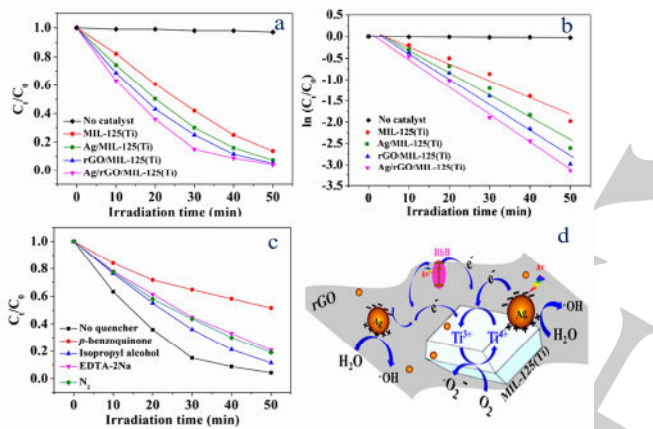


Figure 9- (a) RhB degradation photocatalytic performance of MIL-125(Ti), Ag/ MIL-125(Ti), rGO/MIL-125(Ti) and Ag/rGO/MIL-125(Ti). For comparison,photocatalytic performance for no catalyst is also given; (b) Fitting of pseudo first-order linear line for photocatalytic reaction; (c) Effects of various reactive species scavengers on the photodegradation of RhB catalyzed by Ag/rGO/MIL-125(Ti) under visible light irradiation. (d) Schematic of photogenerated charge carrier separation and transfer in the Ag/rGO/MIL-125(Ti) system under visible light irradiation,^[117g] Copyright (2016) John Wiley & Sons, Ltd.

Carbon nitride ($\text{g-C}_3\text{N}_4$) is another metal-free semiconductor with two-dimensional planar π conjugation structure that bears strong covalent C–N bonds instead of C–C bonds in each layer, while the layers are bound by van der Waals forces, only.^[27b, 122] Its easy preparation from the condensation of simple nitrogen-rich precursors, low cost and sustainable properties allow $\text{g-C}_3\text{N}_4$ predominantly attractive for solar energy utilization. Moreover, the $\text{g-C}_3\text{N}_4$ has a mid-wide band gap (~2.7 eV) with the level of CB and VB of about -1.3 eV and 1.4 eV, respectively, which enables it to absorb light over a wide range of wavelengths and facilitates visible light catalytic reaction.^[6d, 117i] Benefiting from the excellent electronic

conductivity of π conjugated structure, the incorporation of $\text{g-C}_3\text{N}_4$ into various photocatalysts imparted them with improved charge carrier separation and transportation and prolonged the charge carrier lifetime.^[7d] Therefore some researchers have synthesized many $\text{g-C}_3\text{N}_4$ /MOFs nanocomposites to improve photocatalytic properties towards dyes degradation under visible-light irradiation.^[27b, 117i] For example, Guo and coworkers have facile synthesized the $\text{g-C}_3\text{N}_4/\text{MIL-53(Al)}$ composite in DMF at room temperature for RhB degradation under visible-light irradiation. It is found that the photocatalytic degradation rate for $\text{g-C}_3\text{N}_4/\text{MIL-53(Al)}$ is sensitive to $\text{g-C}_3\text{N}_4$ loading, and $\text{g-C}_3\text{N}_4/\text{MIL-53(Al)}$ with a $\text{g-C}_3\text{N}_4$ weight ratio of 20% (~100% after 75min) has the highest efficiency. After the fifth run, the photocatalytic activity of $\text{g-C}_3\text{N}_4$ (20 wt%)/MIL-53(Al) retains over 90% of its original value.^[27b] Under light irradiation, the e^- are excited and h^+ are generated on CB and VB of $\text{g-C}_3\text{N}_4$ respectively. Then, the e^- in the CB of $\text{g-C}_3\text{N}_4$ migrates to the CB of MIL-53(Al) due to that the interfacial contact formed between $\text{g-C}_3\text{N}_4$ and MIL-53(Al) effectively hinders the recombination of e^- - h^+ pairs. Subsequently, the accumulated e^- and h^+ are transformed to the reactive species for RhB degradation.^[27b] In addition, Wang and coworkers have prepared $\text{g-C}_3\text{N}_4/\text{MIL-125(Ti)}$ (CMTi) nanocomposite which assembles through strong $\pi-\pi$ interactions and Ti-N bands by solvothermal route.^[117i] After incorporation, the visible-light responses of CMTi composite are significantly improved, and the CMTi-2 has a lowest E_g value of 3.24 than that of other samples (Figure 10a). The synergistic effect between MIL-125(Ti) and $\text{g-C}_3\text{N}_4$ is confirmed by the RhB photodegradation that all of CMTi hybrids exhibit higher photocatalytic activity than that of both MIL-125(Ti) and $\text{g-C}_3\text{N}_4$ benifiting from effective charge transfer at heterointerfaces and the enhanced quantum efficiency (Figure 10b). The RhB degradation depends on both holes (h^+) and $\cdot\text{O}_2^-$ greatly compared with $\cdot\text{OH}$ radical and O_2 is the main factor affecting the formation of $\cdot\text{O}_2^-$ (Figure 10c). As shown in Figure 10d, the CMTi-2 can be reused for five runs without distinct photocorrosion. During the photocatalytic process, the electrons can be generated from RhB and $\text{g-C}_3\text{N}_4$ and then electrons participate in reversible transformation between Ti^{4+} and Ti^{3+} for radicals generation (Figure 10e).^[117i]

Conducting organic polymers have been extensively investigated for their remarkable electrical and optoelectronic properties.^[100, 118d] The extended π -electron system of organic polymers imparts them high stability and high mobility charge carriers, which are desirable to achieve enhanced photocatalytic activity by integrating them with other functional materials. One of the most studied polymers is polyaniline (PANI) ($E_g = 2.8 \text{ eV}$) which has attracted wide attention for the synthesis of composites/blends and copolymers to improve their processability^[33]. For example, both Wang and Cui groups have loaded the polyaniline (PANI) on the Cd^{II} MOFs for the fabrication of PANI/[CdL] \cdot [$\text{H}_2\text{N}(\text{CH}_3)_2$](DMF)(H₂O)₃ and PANI/[Cd(dcbpyno)(bix)_{1.5}]·2H₂O, respectively. The great enhanced photocatalytic performances for RhB of PANI/[CdL] \cdot [$\text{H}_2\text{N}(\text{CH}_3)_2$](DMF)(H₂O)₃ and PANI/[Cd(dcbpyno)(bix)_{1.5}]·2H₂O are observed due to the

strong photoresponse of PANI in the visible-light region as well as high quantum yields. [33, 80] Under visible light, only PANI can be excited and produce electrons on its LUMO, then the electrons transfers into the CB of MOFs, which leads to effective separation of e^-h^+ pairs and hinders their recombination. The resulting electrons and holes can further produce $\cdot O_2^-$ and $\cdot OH$ for the RhB destruction. Similar mechanism is reproposed by Xu with the PPy/ZnP₂Mo₅NR (ppy = polypyrrole) and [Cu2Br(ptz)]n/Carbon fiber (ptz=5-(4-pyridyl)-1H-tetrazole) for RhB degradation. The PPy/ZnP₂Mo₅NRs is prepared via a facile in situ chemical oxidation polymerization process under the initiation of ammonium persulfate (APS) and [Cu2Br(ptz)]n/Carbon fiber is synthesized through a colloidal blending process. Under visible light irradiation, both of them exhibit high photocatalytic activity compared to parents attributing to the synergistic effect profiting from high separation efficiency of the photogenerated electrons and holes on the interface of MOFs and Ppy or carbon fiber. [118d, 118e]

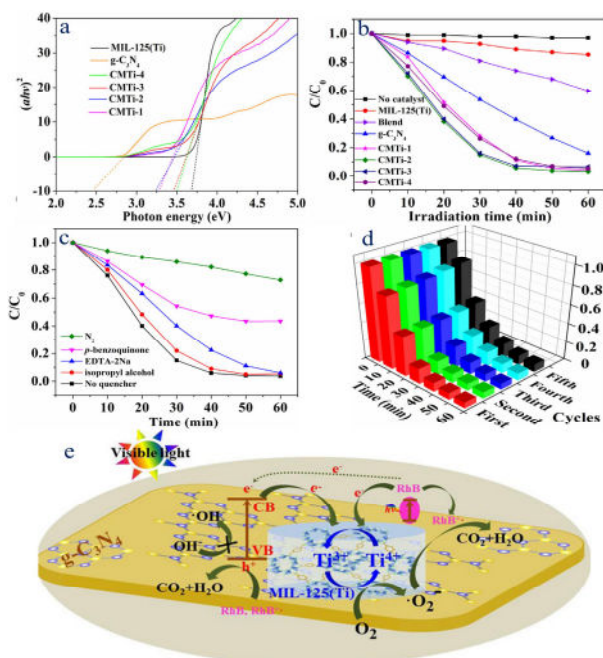


Figure 10- (a) The plot of $(ahv)^2$ vs. photon energy ($h\nu$) of CMTi composite; (b) RhB degradation photocatalytic performance of g-C₃N₄, MIL-125(Ti) and CMTi composites. For comparison, photocatalytic performance for no catalyst is also given. The “Blend” represents the sample of mechanically blending of MIL-125(Ti) and g-C₃N₄ with the g-C₃N₄ content of 7 wt%; (c) Effects of different reactive species scavengers on the photodegradation of RhB by CMTi-2 under visible-light irradiation; (c) Recycling tests of CMTi-2 under solar light irradiation; (e) Schematic of photo-generated charge carrier's separation and transfer in the CMTi system under visible-light irradiation [117]. Copyright (2015) Elsevier.

4. MOFs derived photocatalysts

Due to the highly ordered porous structures with abundant organic struts, MOFs would be good candidates for using as precursors to fabricate photoactive semiconductors or their

composite under suitable calcination conditions. [123] Comparing with general synthesis methods, this strategy not only avoid the need for a template and complex apparatus but also exhibits ability to control the shape of the target products. [124] By selecting the appropriate precursor coupled with a rational calcination procedure, products with unique sizes and shapes could be obtained. This method also has potential advantages, including operational simplicity, high yield of pure products, absence of solvent, low energy consumption and functional efficiency, exempting the need for special equipment. [125] The photocatalytic performance of as-prepared nanostructured metals (metal oxides, metal sulfide or their hybrid) depends on the morphologies of MOFs and synthesis conditions, such as temperature, post-treatment and so on.

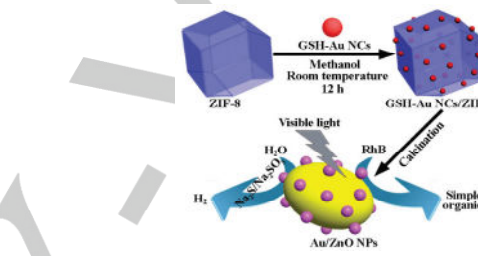


Figure 11- Schematic representation of the synthetic route for the controllable fabrication of the rhombic dodecahedral GSH-Au NCs/ZIF-8NPs and their derived Au/ZnO NPs for the visible light photocatalytic hydrogen production together with degradation of RhB. [126] Copyright (2014) Royal Society of Chemistry.

As shown in Table 5, some of MOFs derived photocatalysts are developed for dye degradation. [28b, 127] For examples, the commonly used photocatalysts of TiO₂ and ZnO are prepared by hydrothermal and thermal treatment of Ti₂O₃(H₂O)₂(C₂O₄)·H₂O and ZIF-8(Zn), respectively. Based on the chemical advanced oxidation assistance, the degradation of chromotrope FB(CFB) by TiO₂ is 60% after 7.5 h UV-Visible irradiation. [127f] Compared with TiO₂, the ZnO shows more efficiency in MB decomposition. It is found that the calcination temperature or time significantly influences the photocatalytic activity, and the photocatalytic activity follows the order: ZnO-500-5 (Temperature 500 °C and time 5 h) > ZnO-700-5 > ZnO-300-3 > ZnO-300-5. However, the photocatalytic efficiency is also not very satisfactory. The degradation degree of MB by ZnO-500-5 is 76% after 60 min of irradiation. [127g] To improve the photocatalytic performance, the ternary metal oxides of CoFe₂O₄ with MB degradation of 92% under 7 h visible light irradiation is prepared based on the thermolysis of metal-NN complexes by Tavana and coworkers. [128] The GdCoO₃ with size of 3, 12, and 200 nm are obtained by Mahata and accompaniers via calcining the [Gd(H₂O)₃Co(C₅N₁H₃(COO)₂)₃] in air for 10 h at three different temperatures of 400, 700, and 800 °C, respectively. Among them, the 3 nm GdCoO₃ shows more active in degrading the RhB, Rhodamine Blue (RBL), Orange G (OG), and Remazol Brilliant Blue R (RBBR). [129]

Composite hybrid nanostructures formed from noble metals especially for Au and semiconductor NPs have attracted great attention for their enhanced or even new functionalities. He and coworkers have fabricated the Au/ZnO NPs, which is derived from the calcination of yellow fluorescent glutathione-Au nanoclusters/zeolitic imidazolate framework-8 nanoparticles (GSH-Au NCs/ZIF-8 NPs) (Figure 11). [126] The Au/ZnO NPs present excellent visible light photocatalytic degradation of RhB. During the photocatalytic process, the electrons could be photoexcited from ZnO and then transfer to Au, which is driven by the energy gap between CB with higher energy level of ZnO and the new Fermi energy level of Au/ZnO. The Au NPs act as the container for photo-generated electrons and induce a shift

of the Fermi level toward more negative potentials until the Fermi level reaches near to the CB of ZnO. Thus, the recombination of photoelectrons and holes is prevented and the photo-induced generation of electron-hole pairs will continue. Meanwhile, when plasmonic-Au NPs absorb visible light, the electrons near the Fermi level are excited to the surface plasmon resonance (SPR) state, injected into the CB of the ZnO NPs and then participate in the photocatalytic reactions. Therefore, under appropriate visible light irradiation, the photocatalytic activities of Au/ZnO NPs could be greatly boosted. [126]

Table 5 Performance of some Metal-organic-framework derived catalysts for the degradation of organic dyes

Derivatives	Precursors (MOF)	E _g (eV)	Dye	Dye and composites concentration (mg·L ⁻¹)	additive	Light/time degradation (min)	for	Removal%	Ref.
Au/ZnO	ZIF-8(Zn)	3.17	RhB	2.4 and 500	None	Vis/240		90 ^a	[126]
Co ₃ O ₄ / GN	ZIF-67(Co)	-	AY	100 and 500	HSO ₅ ⁻	UV/20		82 ^a	[130]
Fe ₂ O ₃ /C	MIL-88A(Fe)	-	RhB	10/333	Na ₂ S ₂ O ₈	UV/80		90 ^a	[131]
ZnO-500-5	ZIF-8(Zn)	3.37	MB	8 and 1000	None	UV/60		76	[127c]
ZnO-7500-5	ZIF-8(Zn)	3.37	MB	8 and 1000	None	UV/60		63 ^a	[127c]
SnS	[Sn(TEA)n] ²⁺ ·2Cl ⁻	1.33	RhB	8 and 200	None	Vis/180		55 ^a	[127e]
TiO _x /C(T ₆)	MIL-125(Ti)	-	MB	20 and 200	None	UV/60		39	[127g]
C/ZnO(C350-400)	ZIF-8(Zn)	2.93 ^a	RhB	9.6 and 200	None	Vis/60		95 ^a	[7b]
C/ZnO(C350-450)	ZIF-8(Zn)	2.97 ^a	RhB	9.6 and 200	None	Vis/60		98 ^a	[7b]
GdCoO ₃	[Gd(H ₂ O) ₃ Co(C ₅ N ₁ H ₃ (COO) ₂) ₃]	-	OG	46.8 and	None	UV/30		100 ^a	[129]
GdCoO ₃	[Gd(H ₂ O) ₃ Co(C ₅ N ₁ H ₃ (COO) ₂) ₃]	-	RRBR	109 and	None	UV/90		85 ^a	[129]
GdCoO ₃	[Gd(H ₂ O) ₃ Co(C ₅ N ₁ H ₃ (COO) ₂) ₃]	-	RB	9.3 and	None	UV/35		100 ^a	[129]
GdCoO ₃	[Gd(H ₂ O) ₃ Co(C ₅ N ₁ H ₃ (COO) ₂) ₃]	-	RBL	13.6 and	None	UV/30		100 ^a	[129]
CuO	C ₂₃ H ₃₄ Cl ₂ Cu ₂ N ₈ O ₆ S ₂	0.98	MB	10 and 2000	H ₂ O ₂	UV/360		96	[127b]
CoFe ₂ O ₄	Fe(C ₁₀ H ₇ NO ₂) ₃ , Co(C ₁₀ H ₇ NO ₂) ₂	2.28	MB	0.4 and 1000	None	Vis/420		92	[128]
In ₂ S ₃	[In(bipy)(SC(O)Ph) ₃]	2.07	MB	7.5 and 25	None	UV/25		44	[28a]
ZnIn ₂ S ₄	[Zn(SC(O)Ph) ₂]·2H ₂ O and [In(bipy)(SC(O)Ph) ₃]	2.30	MB	7.5 and 25	None	UV/25		66	[28a]
CdIn ₂ S ₄	[Cd(SC(O)Ph) ₂]·2H ₂ O and [In(bipy)(SC(O)Ph) ₃]	2.30	MB	7.5 and 25	None	UV/25		51	[28a]
TiO ₂	Ti ₂ O ₃ (H ₂ O) ₂ (C ₂ O ₄)·H ₂ O	-	CFB	100 and 1000	H ₂ O ₂	UV-Vis/450		60	[127f]
ZnO@Silica	ZIF-8(Zn)	-	MO	10 and 200	None	UV/240		95	[127a]
γ -Fe ₂ O ₃ /C	MIL-53(Fe)	-	MG	500 and 2000	H ₂ O ₂	Sunlight/30		100	[28b]

TEA = triethanolamine^[127e]; C₁₀H₇NO₂ = α -nitroso- β -naphthol^[128]; bipy = 2,2'-bipyridyl^[28a]. ^aValues estimated from original figures of the references.

Because of the regular arrangement of metal nodes in MOFs, the carbon hybrids containing uniformly dispersed metal

oxides are prone to be formed in the in situ carbonization the MOFs. The metallic oxide/carbon composites have several

advantages, including higher surface area for adsorption of reagents, extended light absorption range and higher absorption intensity, and longer electron–hole lifetime.^[127f, 127g] In this situation, the TiO_x/C composites with adjustable chemical composition and pore texture are constructed for MB degradation using MIL-125(Ti) as the sacrificial precursors.^[127g] The C-doped cubic ZnO is also successfully synthesized using zeolite imidazolate frameworks (ZIF-8) as the precursor. In the preparation process, the ZIF-8 is first calcined under 350 °C for 2 h to result in the porous structure, then the pyrolysis temperature is increased to 400 °C for 1 h to increase the crystallization of ZnO.^[132] The higher surface area and porous structure benefit reaction/interaction which occurs on the surface or at the interface of ZnO. Under visible-light irradiation, the C350-400 (5.4% C doping) shows 1.2-fold, 1.7-fold and 1.8-fold higher photoactivity than C350-450 (3.6% C doping), C-ZnO (2.7% C doping) and C400 (1.9% C doping) in RhB degradation, respectively (Figure 12a), which is resulted from the enhanced electron-hole separation and optical absorption/mass transfer. Furthermore, the photoactivity trend is the same with that under UV–vis irradiation (Figure 12b) and the C350-400 shows high photostability (Figure 12c) without obvious deactivation after five degradation cycles. Also, the C350-400 shows the highest photoelectrochemical activity with the current density of 83 μA/cm² (Figure 12d). In electrochemical impedance spectroscopy (Figure 12e), the C350-400 and C350-450 show smaller radius than directly calcined samples (C350, C400 and C450). Therefore, charges in the formers can be quickly transferred to reactant through the solid/liquid interface and consumed by chemical reaction, which in turn retards the charge recombination or back charge transfer side processes.^[132]

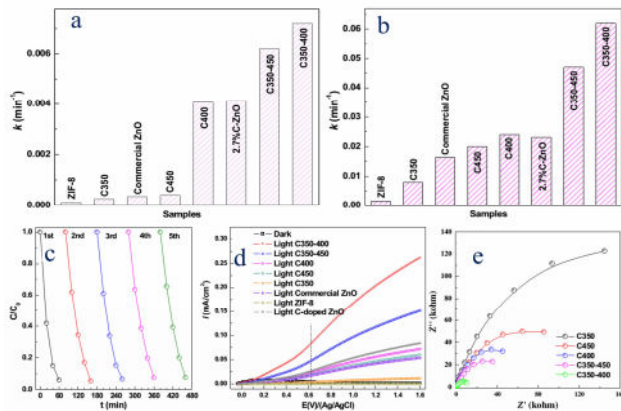


Figure 12. The calculated reaction rates (k) for RhB photodegradation under visible (> 420 nm) light (a) and UV-vis (Xenon light) light (b); the cycling of RhB photodegradation (UV-vis light) over C350-400 (c), current-voltage curve (d) and electrochemical impedance spectroscopy (EIS) of the prepared ZnO (e).^[132] Copyright (2016) Elsevier.

In order to overcome the weakness of difficult separation, many magnetic porous carbon composites are exploited using MOFs precursor. For example, Lin and coworkers have

synthesized the magnetic iron/carbon nanorods (Fe₂O₃/C) and cobalt-graphene (Co₃O₄/GN) by one-step carbonization using MIL-88A and ZIF-67(Co)/graphene oxide, respectively.^[130–131] It is found that both catalysts have excellent UV active for dye degradation (Fe₂O₃/C for RhB and Co₃O₄/GN for acid yellow (AY)) in the presence of H₂O₂, permonosulphate, and/or persulfate. In fact, the magnetic iron materials is a good activator for photofenton and photofenton liked process. Zhang and workmates have utilized the MIL-53(Fe) as a template to fabricated the γ-Fe₂O₃/C composite via a microwave enhanced high-temperature ionothermal method. The application of γ-Fe₂O₃/C for MG degradation in the presence of H₂O₂ indicates that the porous carbon supported on the γ-Fe₂O₃ can improve the degradation reaction rate due to that the porous carbon can adsorb the MG from water and narrow MG and the catalyst.^[28b]

Besides the metal oxides and their hybrids synthesized from MOF precursor, the metal sulfide can also be prepared with controllable size, shape, and structure.^[125a] By polyol refluxing the tin(II) chloride, thioacetamide, and triethanolamine in ethylene glycol, the SnS nanoflowers consisting of mesoporous nanoplates composed of nanoparticles are modulated with the formation and array of chelate complex [Sn(TEA)_n]²⁺·2Cl⁻ clusters. Toward RhB degradation, the SnS nanoflowers show higher photocatalytic activities than the SnS nanoparticles, which ascribes to their higher surface area, small crystal sizes and mesoporous hierarchical architectures.^[127e] Due to the unique optoelectronic, optical, and catalytic properties of ternary chalcogenide, the ZnIn₂S₄ and CdIn₂S₄ are prepared using dual-source precursors at 300 °C for 24 h under nitrogen atmosphere. After incorporation of Zn(II) and Cd(II), the photocatalytic properties of ZnIn₂S₄ and CdIn₂S₄ are enhanced comparing with In₂S₃ nanocrystals over the same UV irradiation time. Overall photocatalytic activity depends on the efficiency of photoabsorption, reaction efficiency of photogenerated electron–hole pairs, and their recombination rate.

5. Conclusions and outlooks

Nowadays, the newly emerged crystalline porous materials of MOFs give a promising future to utilize the solar energy for dye wastewater remediation. The ability of light-harvesting by the organic linkers and conversion of the initial ligand-localized exciton into a charge-separate state by single electron transfer from the ligand to the metal nodes have inspired great interest of researchers in photocatalytic degradation of dyes by MOFs. Compared with traditional semiconductor, the photoactive MOFs for wastewater decolorization have several advantages: (1) The diverse synthesis methods including solvothermal, emulsion-assistant precipitation, vapor diffusion and microwave irradiation, provide a high degree of morphology control at the molecular level. (2) The well-defined crystalline structure and intrinsic porosity benefit the mass transfer and diffusion of dyes through the open channels, and characterization. (3) The versatile shapes and functions provide a platform for the construction of composite with other material (i.e. Bi₂O₃, GO, C₃N₄) easy. Incorporating metal NPs and nonmetal materials

within MOFs is an effective way to achieve unique functions originating from the synergistic effect. (4) Using MOFs (tunable pore size) as sacrificial precursors paves the way to design and synthesize metal nanoparticles and metal nanoparticles /carbon composite. It not only avoids the need for a template and complex apparatus but also exhibits ability to control the shape of the target products.

The dye degradation performance of MOFs based materials significantly depends on the optical absorption and charge separation efficiency properties as well as the number of catalytic sites, which relates to the central metals, the structures of the MOFs, the extent of the conjugation, the coordinated environment and the steric hindrance around the active metal centers. The addition of oxidizing agents (i.e. H₂O₂, Na₂S₂O₈) and the coexisting pollutants of Cr(VI) result in a synergistic effect on the photocatalysis of dye. However, the assessing the ability of the photoactive MOFs is only relied on the examination of one of the few dyes, i.e. MB, RhB, MO, and MG degradation by photogenerate reactive transient species (e.g. O₂[•], •OH), which intensively limits the conclusions of the MOFs photocatalytic activity due to the fact that the reactive species are nonselective and can react with a wide variety of substrates. Upon the light illumination, some dyes can self sensitize to produce electrons and then inject the electron into the CB of MOFs based materials to form the active radicals for the dyes degradation or mineralization. In this case, sensitized dye degradation is a fuzzy factor in the assessment of photocatalytic activity. Therefore, it is necessary to quantitatively measure selfsensitization in the photodegradation of dyes by MOFs based materials. Is there an internal relationship between the selfsensitization of dye and selective degradation?

To widely and effectively utilize the solar energy in nature, research efforts have focused on construction of MOFs composite to enable absorption of the visible-light region. In comparison, the near-infrared (NIR) light with sufficient proportion in the solar spectrum (~ 44%) remains beyond efficient use. The harnessing of NIR photons is therefore an important challenge for photocatalysis development of MOFs based materials. Fabrication of heterojunctions or hybrids has been proved to be an effective strategy to promote the charge separation in photovoltaics. However, the essential relations of electron transport between the junctions and the photocatalytic activity are far less well understood. Hence, the indepth understanding of charge separation and migration with visual evidence is desirable for efficient MOFs based photocatalysts design. For the purpose realizing the industrialization operation of dye photocatalytic degradation, the scale production of the photocatalyst is essential. Up to date, it is difficult to produce the MOFs in enormous quantities within a relatively short time at ambient condition. The most commonly used method, solvothermal method usually involves the use of an autoclave or reflux condensation, which will take days or weeks to finish a batch of MOFs preparation. Besides, the high reaction-stable of MOFs is desired for the photocatalytic process. Although the Cr³⁺, Fe³⁺, Al³⁺, Ti⁴⁺ and Zr⁴⁺ based MOFs containing donor atoms (O or N) tends to have the satisfactory thermal, chemical

and water stability properties, many other MOFs constructed from carboxylate ligands and Zn²⁺, Cd²⁺ or Co²⁺ cations as SBUs are poor chemical stability. It is expected to improve the stability by optimizing coordination between the metal cluster and the organic linkers, modifying or hybriding with other materials.

All in all, although many challenges still exist, the rapid development of photoactive MOFs based materials has predicted well for a bright future. In particular, with sustained research efforts towards the MOFs composites and their ramifications, the practical application in scale treatment of dye wastewater may eventually be achieved.

Acknowledgements

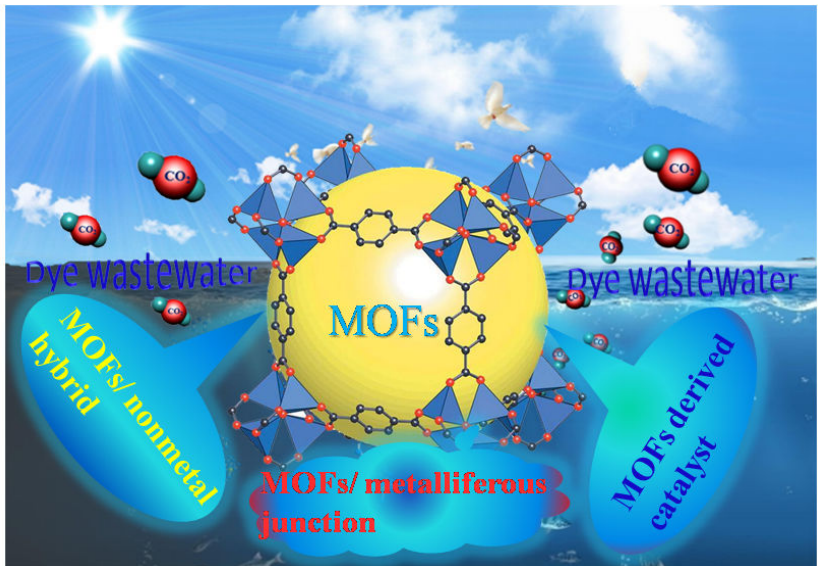
The authors gratefully acknowledge the financial support provided by Collaborative Innovation Center of Resource-Conserving & Environment-friendly Society and Ecological Civilization, the National Natural Science Foundation of China (No. 21276069, 71431006, 51521006)

Keywords: Metal-organic frameworks; Photocatalytic; Dye; Degradation; Wastewater;

- [1] W.-W. Li, H.-Q. Yu, Z. He, *Energ. Environ. Sci.* **2013**, *7*, 911-924.
- [2] aP. Luo, Y. Zhao, B. Zhang, J. Liu, Y. Yang, J. Liu, *Water. Res.* **2010**, *44*, 1489-1497; bC.-C. Wang, J.-R. Li, X.-L. Lv, Y.-Q. Zhang, G. Guo, *Energ. Environ. Sci.* **2014**, *7*, 2831-2867.
- [3] aJ. Yener, T. Kopac, G. Dogu, T. Dogu, *Chem. Eng. J.* **2008**, *144*, 400-406; bT. K. Saha, H. Frauendorf, M. John, S. Dechert, F. Meyer, *ChemCatChem.* **2013**, *5*, 796-805.
- [4] aZ. Wu, H. Zhong, X. Yuan, H. Wang, L. Wang, X. Chen, G. Zeng, Y. Wu, *Water. Res.* **2014**, *67*, 330-344; bR. Saladino, M. Guazzaroni, C. Crestini, M. Crucianelli, *ChemCatChem.* **2013**, *5*, 1407-1415.
- [5] aL. Ai, J. Jiang, *Chem. Eng. J.* **2012**, *192*, 156-163; bL. Leng, X. Yuan, H. Huang, J. Shao, H. Wang, X. Chen, G. Zeng, *Appl. Surf. Sci.* **2015**, *346*, 223-231.
- [6] aL. Zhang, X. Yuan, H. Wang, X. Chen, Z. Wu, Y. Liu, S. Gu, Q. Jiang, G. Zeng, *RSC Adv.* **2015**, *5*, 98184–98193; bE. Brillas, C. A. Martínez-Huitle, *Appl. Catal. B: Environ.* **2015**, *166-167*, 603-643; cL.-j. Leng, X.-z. Yuan, H.-j. Huang, H. Wang, Z.-b. Wu, L.-h. Fu, X. Peng, X.-h. Chen, G.-m. Zeng, *Fuel. Process. Techn.* **2015**, *129*, 8-14; dH. Wang, X. Yuan, H. Wang, X. Chen, Z. Wu, L. Jiang, W. Xiong, G. Zeng, *Appl. Catal. B: Environ.* **2016**, *193*, 36-46.
- [7] aM. N. Chong, B. Jin, C. W. Chow, C. Saint, *Water. Res.* **2010**, *44*, 2997-3027; bS. Gu, Y. Chen, X. Yuan, H. Wang, X. Chen, Y. Liu, Q. Jiang, Z. Wu, G. Zeng, *RSC Adv.* **2015**, *5*, 79556-79564; cY. Liu, X. Yuan, H. Wang, X. Chen, S. Gu, Q. Jiang, Z. Wu, L. Jiang, Y. Wu, G. Zeng, *Catal. Commun.* **2015**, *70*, 17-20; dH. Wang, X. Yuan, H. Wang, X. Chen, Z. Wu, L. Jiang, W. Xiong, Y. Zhang, G. Zeng, *RSC Adv.* **2015**, *5*, 95643-95648; eS. Liu, Z. R. Tang, Y. Sun, J. C. Colmenares, Y. J. Xu, *Chem. Soc. Rev.* **2015**, *44*, 5053-5075.
- [8] aX. Yuan, H. Wang, Y. Wu, X. Chen, G. Zeng, L. Leng, C. Zhang, *Catal. Commun.* **2015**, *61*, 62-66; bQ. Jiang, X. Yuan, H. Wang, X. Chen, S. Gu, Y. Liu, Z. Wu, G. Zeng, *RSC Adv.* **2015**, *5*, 53019-53024; cX. Chen, S. S. Mao, *Chemical review* **2007**, *107*, 2891-2959; dY. Liu, X. Yuan, H. Wang, X. Chen, S. Gu, Q. Jiang, Z. Wu, L. Jiang, G. Zeng, *RSC Adv.* **2015**, *5*, 33696-33704.
- [9] aC. Chen, W. Ma, J. Zhao, *Chem. Soc. Rev.* **2010**, *39*, 4206-4219; bZ. Zheng, J. Zhao, H. Liu, J. Liu, A. Bo, H. Zhu, *ChemCatChem.* **2013**, *5*, 2382-2388.
- [10] X. Pan, M. Q. Yang, X. Fu, N. Zhang, Y. J. Xu, *Nanoscale.* **2013**, *5*, 3601-3614.
- [11] aH. Wang, X. Yuan, Y. Wu, G. Zeng, H. Dong, X. Chen, L. Leng, Z. Wu, L. Peng, *Appl. Catal. B: Environ.* **2016**, *186*, 19-29; bB. T. Yonemoto, G. S. Hutchings, F. Jiao, J. Am. Chem. Soc. **2014**, *136*, 8895-8898; cY. Shi, Y. Chen, G. Tian, L. Wang, Y. Xiao, H. Fu, *ChemCatChem.* **2015**, *7*, 1684-1690.

- [12] aH. Huang, J. R. Li, K. Wang, T. Han, M. Tong, L. Li, Y. Xie, Q. Yang, D. Liu, C. Zhong, *Nat. Commun.* **2015**, *6*, 8847; bD. Feng, K. Wang, Z. Wei, Y. P. Chen, C. M. Simon, R. K. Arvapally, R. L. Martin, M. Bosch, T. F. Liu, S. Fordham, D. Yuan, M. A. Omary, M. Haranczyk, B. Smit, H. C. Zhou, *Nat. Commun.* **2014**, *5*, 5723; cA. J. Howarth, Y. Liu, P. Li, Z. Li, T. C. Wang, J. T. Hupp, O. K. Farha, *Nat. Rev. Mater.* **2016**, *1*, 15018.
- [13] aZ. Wu, X. Yuan, H. Zhong, H. Wang, G. Zeng, X. Chen, H. Wang, L. Zhang, J. Shao, *Sci. Rep.* **2016**, *6*, 25638; bS.-L. Xiao, Y.-H. Li, P.-J. Ma, G.-H. Cui, *Inorg. Chem. Commun.* **2013**, *37*, 54-58.
- [14] aJ.-L. Wang, C. Wang, W. Lin, *ACS Catal.* **2012**, *2*, 2630-2640; bT. Zhang, W. Lin, *Chem. Soc. Rev.* **2014**, *43*, 5982-5993.
- [15] aH. S. Quah, W. Chen, M. K. Schreyer, H. Yang, M. W. Wong, W. Ji, J. J. Vittal, *Nat. Commun.* **2015**, *6*, 7954; bP. C. Banerjee, D. E. Lobo, R. Middag, W. K. Ng, M. E. Shaibani, M. Majumder, *ACS Appl. Mater. Interfaces* **2015**, *7*, 3655-3664.
- [16] T. M. McDonald, J. A. Mason, X. Kong, E. D. Bloch, D. Gygi, A. Dani, V. Crocelia, F. Giordanino, S. O. Odoh, W. S. Drisdell, B. Vlaisavljevich, A. L. Dzubak, R. Poloni, S. K. Schnell, N. Planas, K. Lee, T. Pascal, L. F. Wan, D. Prendergast, J. B. Neaton, B. Smit, J. B. Kortright, L. Gagliardi, S. Bordiga, J. A. Reimer, J. R. Long, *Nature* **2015**, *519*, 303-308.
- [17] S. T. Meek, J. A. Greathouse, M. D. Allendorf, *Adv. Mater.* **2011**, *23*, 249-267.
- [18] aS. Wang, X. Wang, *Small* **2015**, *11*, 3097-3112; bM. A. Nasalevich, M. G. Goesten, T. J. Savenije, F. Kapteijn, J. Gascon, *Chem. Commun.* **2013**, *49*, 10575-10577.
- [19] L. Ai, C. Zhang, L. Li, J. Jiang, *Appl. Catal. B: Environ.* **2014**, *148-149*, 191-200.
- [20] aH. Wang, X. Yuan, Y. Wu, X. Chen, L. Leng, G. Zeng, *RSC Adv.* **2015**, *5*, 32531-32535; bH. Wang, X. Yuan, Y. Wu, G. Zeng, X. Chen, L. Leng, Z. Wu, L. Jiang, H. Li, *J. Hazard. Mater.* **2015**, *286*, 187-194.
- [21] aY. An, H. Li, Y. Liu, B. Huang, Q. Sun, Y. Dai, X. Qin, X. Zhang, *J. Solid. State. Chem.* **2016**, *233*, 194-198; bY.-P. Yuan, L.-S. Yin, S.-W. Cao, G.-S. Xu, C.-H. Li, C. Xue, *Appl. Catal. B: Environ.* **2015**, *168-169*, 572-576; cJ. Tian, Z. Y. Xu, D. W. Zhang, H. Wang, S. H. Xie, D. W. Xu, Y. H. Ren, H. Wang, Y. Liu, Z. T. Li, *Nat. Commun.* **2016**, *7*, 11580.
- [22] Y. Fu, D. Sun, Y. Chen, R. Huang, Z. Ding, X. Fu, Z. Li, *Angew. Chem. Int. Ed. Engl.* **2012**, *51*, 3364-3367.
- [23] aE. M. Dias, C. Petit, *J. Mater. Chem. A* **2015**, *3*, 22484-22506; bT. L. Doan, H. L. Nguyen, H. Q. Pham, N. N. Pham-Tran, T. N. Le, K. E. Cordova, *Chem. Asian. J.* **2015**, *10*, 2660-2668.
- [24] Z. Sha, J. Sun, H. S. O. Chan, S. Jaenicke, J. Wu, *ChemPlusChem* **2015**, *80*, 1321-1328.
- [25] X. He, K. Fang, X. H. Guo, J. Han, X. P. Lu, M. X. Li, *Dalton. Trans.* **2015**, *44*, 13545-13549.
- [26] Q. L. Zhu, Q. Xu, *Chem. Soc. Rev.* **2014**, *43*, 5468-5512.
- [27] aZ. Sha, H. S. Chan, J. Wu, *J. Hazard. Mater.* **2015**, *299*, 132-140; bD. Guo, R. Wen, M. Liu, H. Guo, J. Chen, W. Weng, *Appl. Organomet. Chem.* **2015**, *29*, 690-697.
- [28] aS. K. Batabyal, S. E. Lu, J. J. Vittal, *Cryst. Growth. Des.* **2016**, *16*, 2231-2238; bC. Zhang, F. Ye, S. Shen, Y. Xiong, L. Su, S. Zhao, *RSC Adv.* **2015**, *5*, 8228-8235.
- [29] aC.-C. Wang, X.-D. Du, J. Li, X.-X. Guo, P. Wang, J. Zhang, *Appl. Catal. B: Environ.* **2016**, *193*, 198-216; bT. R. Cook, Y. R. Zheng, P. J. Stang, *Chem. Rev.* **2013**, *113*, 734-777; cA. Corma, H. Garcia, F. X. Llabres i Xamena, *Chemical review* **2010**, *110*, 4606-4655; dL. Shen, R. Liang, L. Wu, *Chin. J. Catal.* **2015**, *36*, 2071-2088; eH. Zhang, G. Liu, L. Shi, H. Liu, T. Wang, J. Ye, *Nano. Energy* **2016**, *22*, 149-168.
- [30] H. Yang, X.-W. He, F. Wang, Y. Kang, J. Zhang, *J. Mater. Chem.* **2012**, *22*, 21849-21851.
- [31] C.-F. Zhang, L.-G. Qiu, F. Ke, Y.-J. Zhu, Y.-P. Yuan, G.-S. Xu, X. Jiang, *J. Mater. Chem. A* **2013**, *1*, 14329.
- [32] L. Shen, W. Wu, R. Liang, R. Lin, L. Wu, *Nanoscale* **2013**, *5*, 9374-9382.
- [33] Z. Cui, J. Qi, X. Xu, *Inorg. Chem. Commun.* **2013**, *35*, 260-264.
- [34] A. Martínez-de la Cruz, S. M. G. Marcos Villarreal, L. M. Torres-Martínez, E. López Cuéllar, U. Ortiz Méndez, *Mater. Chem. Phys.* **2008**, *112*, 679-685.
- [35] A. Martínez-de la Cruz, S. Obregón Alfaro, E. López Cuéllar, U. Ortiz Méndez, *Catal. Today* **2007**, *129*, 194-199.
- [36] aX. Wang, Z. Chang, H. Lin, A. Tian, G. Liu, J. Zhang, *Dalton. Trans.* **2014**, *43*, 12272; bX. Zhang, L. Fan, W. Fan, B. Li, X. Zhao, *CrystEngComm.* **2015**, *17*, 6681-6692; cS. E. Etaiw, D. I. Saleh, *Spectrochim. Acta. A* **2014**, *117*, 54-60; dH. F. Hao, W. Z. Zhou, H. Y. Zang, H. Q. Tan, Y. F. Qi, Y. H. Wang, Y. G. Li, *Chem. Asian. J.* **2015**, *10*, 1676-1683.
- [37] aW. T. Xu, L. Ma, F. Ke, F. M. Peng, G. S. Xu, Y. H. Shen, J. F. Zhu, L. G. Qiu, Y. P. Yuan, *Dalton. Trans.* **2014**, *43*, 3792-3798; bZ. Chen, J. Lv, K. Yu, H. Zhang, C. Wang, C. Wang, B. Zhou, *J. Coord. Chem.* **2016**, *69*, 39-47.
- [38] S. Bala, S. Bhattacharya, A. Goswami, A. Adhikary, S. Konar, R. Mondal, *Cryst. Growth. Des.* **2014**, *14*, 6391-6398.
- [39] R. Ghosh, A. K. S, S. M. Pratik, A. Datta, R. Nath, S. Mandal, *RSC Adv.* **2014**, *4*, 21195.
- [40] X.-L. Hao, Y.-Y. Ma, Y.-H. Wang, H.-Y. Zang, Y.-G. Li, *CrystEngComm.* **2014**, *16*, 10017-10027.
- [41] X.-L. Hao, Y.-Y. Ma, Y.-H. Wang, W.-Z. Zhou, Y.-G. Li, *Inorg. Chem. Commun.* **2014**, *41*, 19-24.
- [42] Y. N. Hou, Z. N. Wang, F. Y. Bai, Q. L. Guan, X. Wang, R. Zhang, Y. H. Xing, *RSC Adv.* **2014**, *4*, 21180.
- [43] Q. Lan, Z. M. Zhang, Y. G. Li, Y. Lu, E. B. Wang, *Dalton. Trans.* **2014**, *43*, 16265-16269.
- [44] D.-X. Li, C.-Y. Ni, M.-M. Chen, M. Dai, W.-H. Zhang, W.-Y. Yan, H.-X. Qi, Z.-G. Ren, J.-P. Lang, *CrystEngComm.* **2014**, *16*, 2158.
- [45] S. Li, H. Ma, H. Pang, L. Zhang, Z. Zhang, *New J. Chem.* **2014**, *38*, 4963-4969.
- [46] L. Liu, J. Ding, C. Huang, M. Li, H. Hou, Y. Fan, *Cryst. Growth. Des.* **2014**, *14*, 3035-3043.
- [47] L. Liu, J. Ding, M. Li, X. Lv, J. Wu, H. Hou, Y. Fan, *Dalton. Trans.* **2014**, *43*, 12790-12799.
- [48] X. Wang, C. Gong, Y. Qu, G. Liu, J. Zhang, *Chem. Res. Chinese. U.* **2014**, *30*, 709-714.
- [49] X.-L. Wang, Y. Qu, G.-C. Liu, J. Luan, H.-Y. Lin, X.-M. Kan, *Inorg. Chim. Acta* **2014**, *412*, 104-113.
- [50] Q. Zhang, D. Chen, X. He, S. Huang, J. Huang, X. Zhou, Z. Yang, J. Li, H. Li, F. Nie, *CrystEngComm.* **2014**, *16*, 10485-10491.
- [51] A. Chouhana, P. Mayerb, A. Pandey, *Indian. J. Chem.* **2015**, *54A*, 851-857.
- [52] L. Cui, X. Meng, Y. Fan, X. Li, C. Bi, *J. Inorg. Organome. P.* **2015**, *25*, 1490-1494.
- [53] L. Fan, W. Fan, B. Li, X. Zhao, X. Zhang, *CrystEngComm.* **2015**, *17*, 9413-9422.
- [54] Q. Lan, Z.-M. Zhang, Y.-G. Li, E.-B. Wang, *RSC Adv.* **2015**, *5*, 44198-44203.
- [55] D.-X. Li, Z.-G. Ren, D. J. Young, J.-P. Lang, *Eur. J. Inorg. Chem.* **2015**, *2015*, 1981-1988.
- [56] X. Li, L. Yang, C. Qin, F.-H. Liu, L. Zhao, K.-Z. Shao, Z.-M. Su, *RSC Adv.* **2015**, *5*, 59093-59098.
- [57] X.-Y. Li, L. Gao, Y.-Q. Niu, C.-B. Liu, G.-B. Che, Y.-S. Yan, Q.-F. Guan, *J. Inorg. Organome. P.* **2015**, *25*, 886-891.
- [58] H. Lin, H. Lu, M. A. O. Le, J. Luan, X. Wang, G. Liu, *J. Chem. Sci.* **2015**, *127*, 1275-1285.
- [59] X.-X. Lu, Y.-H. Luo, C. Lu, X. Chen, H. Zhang, *J. Solid. State. Chem.* **2015**, *232*, 123-130.
- [60] C.-C. Wang, H.-p. Jing, P. Wang, S.-j. Gao, *J. Mol. Struct.* **2015**, *1080*, 44-51.
- [61] C.-C. Wang, Y.-Q. Zhang, T. Zhu, X.-Y. Zhang, P. Wang, S.-J. Gao, *Polyhedron* **2015**, *90*, 58-68.
- [62] F. Wang, F.-L. Li, M.-M. Xu, H. Yu, J.-G. Zhang, H.-T. Xia, J.-P. Lang, *J. Mater. Chem. A* **2015**, *3*, 5908-5916.
- [63] F. Wang, C. Wang, Z. Yu, Q. He, X. Li, C. Shang, Y. Zhao, *RSC Adv.* **2015**, *5*, 70086-70093.
- [64] H. Wang, X.-Y. Zhang, C.-F. Bi, Y.-H. Fan, X.-M. Meng, *Transit. Metal. Chem.* **2015**, *40*, 769-777.
- [65] X. Wang, Z. Chang, H. Lin, A. Tian, G. Liu, J. Zhang, D. Liu, *RSC Adv.* **2015**, *5*, 14020-14026.
- [66] X. Wang, N. Chen, G. Liu, A. T. X. Sha, K. Ma, *Inorg. Chim. Acta* **2015**, *432*, 128-135.
- [67] X.-L. Wang, C.-H. Gong, J.-W. Zhang, G.-C. Liu, X.-M. Kan, N. Xu, *CrystEngComm.* **2015**, *17*, 4179-4189.
- [68] X.-L. Wang, D.-N. Liu, H.-Y. Lin, G.-C. Liu, X. Rong, *J. Clust. Sci.* **2015**, *27*, 169-181.
- [69] S. Y. Wei, G. Song, F. Bai, Z. Shi, Y.-H. Xing, *ChemPlusChem* **2015**, *80*, 1007-1013.
- [70] R. X. Yao, R. Hailili, X. Cui, L. Wang, X. M. Zhang, *Dalton. Trans.* **2015**, *44*, 3410-3416.
- [71] X.-L. Wang, N.-L. Chen, G.-C. Liu, H.-Y. Lin, J.-W. Zhang, *Eur. J. Inorg. Chem.* **2015**, *2015*, 1924-1940.
- [72] M. Le, J. Luan, X. Zhao, T. Tang, P. Chen, G. Liu, H. Lin, *Chem. Res. Chinese. U.* **2016**, *32*, 8-15.
- [73] F. Wang, C. Wang, Z. Yu, K. Xu, X. Li, Y. Fu, *Polyhedron* **2016**, *105*, 49-55.
- [74] H. Wang, X. Meng, C. Fan, Y. Fan, C. Bi, *J. Mol. Struct.* **2016**, *1107*, 25-30.
- [75] C. Zhang, D. Ma, X. Zhang, J. Ma, L. Liu, X. Xu, J. *Coord. Chem.* **2016**, *69*, 985-995.
- [76] K. K. Bisht, Y. Rachuri, B. Parmar, E. Suresh, *J. Solid. State. Chem.* **2014**, *213*, 43-51.
- [77] K. K. Bisht, Y. Rachuri, B. Parmar, E. Suresh, *RSC Adv.* **2014**, *4*, 7352.

- [78] S.-S. Guo, Z.-L. Wang, G.-W. Xu, Y.-P. Wu, D.-S. Li, *Inorg. Chem. Commun.* **2014**, *49*, 143-146.
- [79] L.-J. Li, L.-K. Yang, Z.-K. Chen, Y.-Y. Huang, B. Fu, J.-L. Du, *Inorg. Chem. Commun.* **2014**, *50*, 62-64.
- [80] F. Wang, C. Dong, Z. Wang, Y. Cui, C. Wang, Y. Zhao, G. Li, *Eur. J. Inorg. Chem.* **2014**, *2014*, 6239-6245.
- [81] H. An, Y. Hu, L. Wang, E. Zhou, F. Fei, Z. Su, *Cryst. Growth. Des.* **2015**, *15*, 164-175.
- [82] Y. L. Hou, S. X. Li, R. W. Sun, X. Y. Liu, S. Weng Ng, D. Li, *Dalton. Trans.* **2015**, *44*, 17360-17365.
- [83] H.-H. Li, X.-H. Zeng, H.-Y. Wu, X. Jie, S.-T. Zheng, Z.-R. Chen, *Cryst. Growth. Des.* **2015**, *15*, 10-13.
- [84] R. Liang, F. Jing, L. Shen, N. Qin, L. Wu, *J. Hazard. Mater.* **2015**, *287*, 364-372.
- [85] L. Liu, D. Wu, B. Zhao, X. Han, J. Wu, H. Hou, Y. Fan, *Dalton. Trans.* **2015**, *44*, 1406-1411.
- [86] S. Ou, J. P. Zheng, G. Q. Kong, C. D. Wu, *Dalton. Trans.* **2015**, *44*, 7862-7869.
- [87] S. Pu, L. Xu, L. Sun, H. Du, *Inorg. Chem. Commun.* **2015**, *52*, 50-52.
- [88] Z. Shao, C. Huang, X. Han, H. Wang, A. Li, Y. Han, K. Li, H. Hou, Y. Fan, *Dalton. Trans.* **2015**, *44*, 12832-12838.
- [89] S. Y. Wei, J. L. Wang, C. S. Zhang, X.-T. Xu, X. X. Zhang, J. X. Wang, Y.-H. Xing, *ChemPlusChem.* **2015**, *80*, 549-558.
- [90] J. Zhang, C. Wang, W. Chen, H. Lin, Y. Wang, C. Zhang, *Transit. Metal. Chem.* **2015**, *40*, 405-412.
- [91] J. Zhang, C. Wang, Y. Wang, W. Chen, M. P. Cifuentes, M. G. Humphrey, C. Zhang, *J. Solid. State. Chem.* **2015**, *231*, 230-238.
- [92] J.-Y. Zhang, Y.-Y. Xing, Q.-W. Wang, N. Zhang, W. Deng, E.-Q. Gao, *J. Solid. State. Chem.* **2015**, *232*, 19-25.
- [93] J. Zhao, W.-W. Dong, Y.-P. Wu, Y.-N. Wang, C. Wang, D.-S. Li, Q.-C. Zhang, *J. Mater. Chem. A.* **2015**, *3*, 6962-6969.
- [94] J.-M. Hu, Y.-Q. Zhao, Y. Baoyi, K. Van Hecke, G.-H. Cui, *Z. anorg. allg. Chem.* **2016**, *642*, 41-47.
- [95] Y. Li, G. Hou, J. Yang, J. Xie, X. Yuan, H. Yang, M. Wang, *RSC Adv.* **2016**, *6*, 16395-16403.
- [96] S. Mosleh, M. R. Rahimi, M. Ghaedi, K. Dashtianb, S. Hajati, *RSC Adv.* **2016**, *6*, 17204-17214.
- [97] B. Mu, R.-D. Huang, *CrystEngComm.* **2016**, *18*, 986-999.
- [98] B. Mu, Q. Wang, R.-D. Huang, *RSC Adv.* **2016**, *6*, 12114-12122.
- [99] D. Marcinkowski, M. Walęsa-Chorab, V. Patroniak, M. Kubicki, G. Kędzińska, B. Michalkiewicz, *New J. Chem.* **2014**, *38*, 604-610.
- [100] Y. Q. Sun, J. C. Zhong, L. Ding, Y. P. Chen, *Dalton. Trans.* **2015**, *44*, 11852-11859.
- [101] C. Xu, N. Hedin, H. T. Shi, Z. Xin, Q. F. Zhang, *Dalton. Trans.* **2015**, *44*, 6400-6405.
- [102] A. Wang, Y. Zhou, Z. Wang, M. Chen, L. Sun, X. Liu, *RSC Adv.* **2016**, *6*, 3671-3679.
- [103] X. Y. Xu, Q. C. Chen, Y. D. Yu, X. C. Huang, *Inorg. Chem.* **2016**, *55*, 75-82.
- [104] Y. Wu, H. Luo, H. Wang, *RSC Adv.* **2014**, *4*, 40435-40438.
- [105] aS. Gao, T. Feng, C. Feng, N. Shang, C. Wang, *J. Colloid. Interface. Sci.* **2016**, *466*, 284-290; bR. Kaur, K. Vellingiri, H. Kim K, A. K. Paul, A. Deep, *Chemosphere.* **2016**, *154*, 620-627.
- [106] P. Bhanja, A. Bhaumik, *ChemCatChem.* **2016**, *8*, 1607-1616.
- [107] Z. N. Wang, F. Y. Bai, X. Wang, D. Shang, Y. H. Xing, *Spectrochim. Acta. A.* **2016**, *163*, 73-78.
- [108] N. T. Binh, P. T. Thu, N. T. H. Le, D. M. Tien, H. T. Khuyen, L. T. K. Giang, N. T. Huong, T. D. Lam, *Int. J. Nanotechnol.* **2015**, *12*, 447.
- [109] W. Guo, Z. Chen, C. Yang, T. Neumann, C. Kubel, W. Wenzel, A. Welle, W. Pfleging, O. Shekhah, C. Woll, E. Redel, *Nanoscale.* **2016**, *8*, 6468-6472.
- [110] Z. Sha, J. Sun, H. S. O. Chan, S. Jaenicke, J. Wu, *RSC Adv.* **2014**, *4*, 64977-64984.
- [111] Z. Sha, J. Wu, *RSC Adv.* **2015**, *5*, 39592-39600.
- [112] H. Zhao, L. Qian, H. Lv, Y. Wang, G. Zhao, *ChemCatChem.* **2015**, *7*, 4148-4155.
- [113] N. Mohaghegh, S. Kamrani, M. Tasviri, M. Elahifard, M. Gholami, *J. Mater. Sci.* **2015**, *50*, 4536-4546.
- [114] S. Li, X. Wang, Q. He, Q. Chen, Y. Xu, H. Yang, M. Lu, F. Wei, X. Liu, *Chin. J. Catal.* **2016**, *37*, 367-377.
- [115] D. Buso, J. Jasieniak, M. D. Lay, P. Schiavuta, P. Scopece, J. Laird, H. Amenitsch, A. J. Hill, P. Falcaro, *Small.* **2012**, *8*, 80-88.
- [116] J. Aguilera-Sigalat, D. Bradshaw, *Coordin. Chem. Rev.* **2016**, *307*, 267-291.
- [117] aH. Wang, X. Yuan, Y. Wu, H. Huang, X. Peng, G. Zeng, H. Zhong, J. Liang, M. Ren, *Adv. Colloid. Interface. Sci.* **2013**, *195-196*, 19-40; bH. Wang, X. Yuan, G. Zeng, Y. Wu, Y. Liu, Q. Jiang, S. Gu, *Adv. Colloid. Interface. Sci.* **2015**, *221*, 41-59; cH. Wang, X. Yuan, Y. Wu, X. Chen, L. Leng, H. Wang, H. Li, G. Zeng, *Chem. Eng. J.* **2015**, *262*, 597-606; dH. Wang, X. Yuan, Y. Wu, H. Huang, G. Zeng, Y. Liu, X. Wang, N. Lin, Y. Qi, *Appl. Surf. Sci.* **2013**, *279*, 432-440; eY. Wu, H. Luo, X. Jiang, H. Wang, J. Geng, *RSC Adv.* **2015**, *5*, 4905-4908; fY. Wu, H. Luo, H. Wang, C. Wang, J. Zhang, Z. Zhang, *J. Colloid. Interface. Sci.* **2013**, *394*, 183-191; gX. Yuan, H. Wang, Y. Wu, G. Zeng, X. Chen, L. Leng, Z. Wu, H. Li, *Appl. Organomet. Chem.* **2016**, *30*, 289-296; hX. Yuan, Z. Wu, H. Zhong, H. Wang, X. Chen, L. Leng, L. Jiang, Z. Xiao, G. Zeng, *Environ. Sci. Pollut. Res. Int.* **2016**, *1-15*; iH. Wang, X. Yuan, Y. Wu, G. Zeng, X. Chen, L. Leng, H. Li, *Appl. Catal. B: Environ.* **2015**, *174-175*, 445-454; jN. Zhang, M. Q. Yang, S. Liu, Y. Sun, Y. J. Xu, *Chem. Rev.* **2015**, *115*, 10307-10377.
- [118] aR. Fazaeli, H. Aliyan, R. S. Banavandi, *Russ. J. Appl. Chem.* **2015**, *88*, 169-177; bR. Liang, L. Shen, F. Jing, N. Qin, L. Wu, *ACS Appl Mater Interfaces.* **2015**, *7*, 9507-9515; cZ. Wu, H. Zhong, X. Yuan, H. Wang, L. Wang, X. Chen, G. Zeng, Y. Wu, *Water. Res.* **2014**, *67*, 330-344; dX. Xu, H. Y. Yang, Z. Y. Li, X. X. Liu, X. L. Wang, *Chemistry-A European Journal.* **2015**, *21*, 3821-3830; eX. Xu, X. Gao, T. Lu, X. Liu, X. Wang, J. Mater. Chem. A. **2015**, *3*, 198-206; fM. Q. Yang, Y. J. Xu, *Nanoscale Horiz.* **2016**, *1*, 185-200.
- [119] Y. Wu, H. Luo, L. Zhang, *Environ. Sci. Pollut. Res. Int.* **2015**, *22*, 17238-17243.
- [120] L. Huang, B. Liu, *RSC Adv.* **2016**, *6*, 17873-17879.
- [121] H. Wang, X. Yuan, *Environ. Sci. Pollut. Res. Int.* **2014**, *21*, 1248-1250.
- [122] J. Liu, H. Q. Wang, M. Antonietti, *Chem. Soc. Rev.* **2016**, *45*, 2308-2326.
- [123] aR. Das, P. Pachfule, R. Banerjee, P. Poddar, *Nanoscale.* **2012**, *4*, 591-599; bX. K. Pei, Y. F. Chen, S. Q. Li, S. H. Zhang, X. Feng, J. W. Zhou, B. Wang, *Chin. J. Chem.* **2015**, *34*, 157-174.
- [124] S. Zhang, C. Zhang, Y. Man, Y. Zhu, *J. Solid. State. Chem.* **2006**, *179*, 62-69.
- [125] aJ.-K. Sun, Q. Xu, *Energ. Environ. Sci.* **2014**, *7*, 2071; bQ. Xu, Z. G. Guo, M. Zhang, Z. G. Hu, Y. H. Qian, D. Zhao, *CrystEngComm.* **2016**, *18*, 4046-4052; cM. Goudarzi, M. Bazarganipour, M. Salavati-Niasari, *RSC Adv.* **2014**, *4*, 46517-46520.
- [126] L. He, L. Li, T. Wang, H. Gao, G. Li, X. Wu, Z. Su, C. Wang, *Dalton. Trans.* **2014**, *43*, 16981-16985.
- [127] aA. Ahmed, M. Forster, J. Jin, P. Myers, H. Zhang, *ACS Appl Mater Interfaces.* **2015**, *7*, 18054-18063; bH. M. Aly, M. E. Moustafa, M. Y. Nassar, E. A. Abdelrahman, *J. Mol. Struct.* **2015**, *1086*, 223-231; cY. Du, R. Z. Chen, J. F. Yao, H. T. Wang, *J. Alloy. Compd.* **2013**, *551*, 125-130; dM. Marszewski, M. Jaroniec, *Langmuir.* **2013**, *29*, 12549-12559; eG. Zhang, Z. Fu, Y. Wang, H. Wang, *Adv. Powder. Technol.* **2015**, *26*, 1183-1190; fY. Zhang, Z. A. Qiao, J. Liu, X. Wang, S. Yao, T. Wang, B. Liu, Y. Ma, Y. Liu, Q. Huo, *Dalton. Trans.* **2016**, *45*, 265-270; gZ. Guo, J. K. Cheng, Z. Hu, M. Zhang, Q. Xu, Z. Kang, D. Zhao, *RSC Adv.* **2014**, *4*, 34221-34225.
- [128] J. Tavana, M. Edrisi, *Mater. Res. Express.* **2016**, *3*, 035009.
- [129] P. Mahata, T. Aarthi, G. Madras, S. Natarajan, *J. Phys. Chem. C.* **2007**, *111*, 1665-1674.
- [130] K. Y. A. Lin, F. K. Hsu, L. W. Der, *J. Mater. Chem. A.* **2015**, *3*, 9480-9490.
- [131] K. Y. A. Lin, F. K. Hsu, *RSC Adv.* **2015**, *5*, 50790-50800.
- [132] L. Pan, T. Muhammad, L. Ma, Z.-F. Huang, S. Wang, L. Wang, J.-J. Zou, X. Zhang, *Appl. Catal. B: Environ.* **2016**, *189*, 181-191.

Entry for the Table of Contents**MINIREVIEW**

Zhibin Wu, Xingzhong Yuan*, Jin Zhang,
Hou Wang*, Longbo Jiang, Guangming
Zeng

Page 1.– Page 24.

**Photocatalytic decontamination of
wastewater containing organic dyes
by metal-organic frameworks and
their derivatives**

1. Introduction
2. Pure MOFs photocatalysts
3. MOFs based composites photocatalysts
 - 3.1 MOFs/ metalliferous junction photocatalysts
 - 3.2 MOFs/nonmetal hybrid photocatalysts
4. MOFs derived photocatalysts
5. Conclusions and outlooks